CENTRO DE INVESTIGACIONES
EN OPTICA, A.C.

"GENERATION OF LG VECTOR MODES WITH ULTRAHIGH STABILITY BASED ON COMPLEX AMPLITUDE MODULATION IN AN ON-AXIS CONFIGURATION"

Versión definitiva. Incluye cambios sugeridos por revisores.

Tesis que para obtener el grado de Maestra en Ciencias (Óptica)

Presenta: Gloria Elizabeth Rodríguez García

Director de Tesis: Dr. Carmelo Guadalupe Rosales Guzmán

Vo. Bo.

León · Guanajuato · México
Septiembre de 2023

Acknowledgements

I would like to express my gratitude to CONAHCYT for the financial support that sustained me throughout my graduate program.

I also acknowledge Dr. Raúl Alfonso Vázquez Nava for his generous support that greatly facilitated the completion of this study.

My deepest gratitude and appreciation goes to Dr. Carmelo Guadalupe Rosales Guzmán for his unwavering guidance and dedication during the developing of my project, for believing in me and encouraging me to do my best.

Thanks to the research group of structured light because of sharing your knowledge and for being an inspiration: Dayver, Edgar, Leo and Fernanda. Thanks to my classmates and friends who always give the best of themselves, for helping me and loving us.

Especially I extend my thanks to my parents and brothers for being always there and giving me the necessary support during the course of my postgraduate education to successfully complete each stage of my life. Thank you: José, May-k, Mawas and Ale.

Abstract

by Gloria Elizabeth Rodríguez García

Structured light is a well-established concept in optics and computer vision for several decades, but it has been just over a decade ago that the concept re-emerged as a topic of interest. It involves manipulating light properties like amplitude, polarization, phase, frequency, spin angular momentum (SAM), and orbital angular momentum (OAM) by combining spatial or temporal degrees of freedom (DoFs). In the broader context of optical research, vector beams have emerged as a fascinating and versatile class of structured light. They are characterized by their spatially varying polarization states, which distinguish them from traditional scalar beams. This multifaceted approach to light has led to remarkable applications across fields such as optical tweezers, high-resolution microscopy, and both classical and quantum communications.

This master's degree thesis presents a pioneering technique for generating vector beams using complex amplitude modulation in an on-axis configuration, where the holograms are displayed in a reflective spatial light modulator. The primary focus of this research is to address a critical issue in the field: the stability of vector beams during their generation and propagation. In addition to proposing a novel vector beam generation method, this work introduces a quantitative approach to assess their stability.

As a proof-of-concept and a central part of study reported on this work is the creation of Laguerre-Gaussian (LG) vector beams with the proposed experimental set up. The experimental results presented in this thesis demonstrate the effectiveness of the proposed technique in generating vector beams for which the stability is ensure by the fact that the light that superimposes to generate the beams is following always the same optical path. The holograms used to generate the beams were computed using the Mathlab software. To fully characterize the vector beams generated, the Stoke's polarimetry was used.

Contents

List of Figures

List of Tables

To my little bird Andrea and my life partner Rafael.

Chapter 1

Introduction

Although the idea of controlling the properties of light dates back many centuries, it has been only a little more than two decades ago [1, 2, 3] when the terms *structured light, tailored light, shaped light, sculpted light* were coined to refer to a beam in which the degrees of freedom (DoFs) either in the spatial or temporal domain have been manipulated: amplitude, polarization, phase, frequency, spin angular momentum (SAM), orbital angular momentum (OAM), among others [4, 5]. Structured light is the most generalized form of light and it arises from the non-separable superposition of one or more DoFs [6]. In the consecutive, the terms "structured light", "structured field" and "structured beam" will be used indistinctly to refer light beams that have been intentionally tailored, nevertheless it is worth mentioning that a broad characterization of structured light differentiates between scalar and vector beams depending on the distribution of polarization along the plane transverse to its propagation: homogeneous along the whole plane for the first case, and inhomogenous for the second case [7].

The great interest that has arisen around structured light has contributed to unveil properties, behaviors and applications that may seem impossible several years ago, such as the self-healing property [8] or its orbital angular momentum [9]. In the same manner, thanks to the interest and efforts dedicated to the study of structured light, the field has had an important development [10]. Structured light has found applications in several fields including optical trapping [11], optical metrology [12], high-resolution microscopy [13], as well as classical and quantum communications [14, 15].

Particularly, due to the versatility and potential applications that structured light may have, there has been a great effort in the generation and characterization of structured fields [16]. In this realm, computer-controlled devices such as Spatial light Modulators (SLMs) and Digital Micro-mirror Devices (DMDs) are quite popular partly due to its flexibility to generate light beams with almost any desired shape [5]. In order to codify the shape of the desired field it is important to have a mathematical representation for it, in this context the choice of a coordinate system is relevant when generating structured beams since it allows to specify how polarization and spatial information are going to be manipulated: depending on the coordinate system used to solve the wave equation, the solutions take different forms. Additionally, having a mathematical representation for the beams, allows to describe, characterize, and analyze them in a convenient way. For the case of the beams generated, reported and described in this work, the selected coordinate system was cylindrical, which give raise to Laguerre-like solutions; these solutions

correspond to Laguerre-Gaussian beams. It is deserving of mention that the manipulation of light when using DMDs or SLMs mainly depends on complex amplitude modulation (CAM) which is primarily an optical technique that involves controlling the phase and amplitude of light independently at different points within a two-dimensional space to create complex spatial patterns of light [17].

Finally, but not less important, it should be mentioned that the characterization of the vector beams is crucial to devise the potential applications of the generated beams, among the quantities to characterize, their 'purity' and 'stability' are outstanded as important parameters to consider. Concerning the purity, there has been a relatively recent but robust formulation that includes the work of McLaren et al [18], Ndgano [19], and Selyem et al [20]; with regard to the stability, the approaches are commonly based on qualitative descriptions but the proposal of Perez-Garcia and collaborators [21] is an attempt of quantifying this property using the root mean squared error.

This thesis is structured into seven chapters to systematically explore this subject as follows:

1. First of all, in chapter 2, the main concepts related with vector beams are shown and a brief explanation about how they differ from scalar beams is provided. In this chapter the paraxial Helmholtz equation as well as its solution in cylindrical coordinates is introduced, followed by the description of the most common vector beam generation techniques, finalizing with the explanation of Stokes formalism and how it can be used to characterize the quality and stability of vector beams.

2. Chapter 3 contains the main information concerning liquid-crystals properties and spatial light modulators characteristics. In the same manner, some techniques that use one or two SLMs to modulate phase, amplitude and polarization, are presented and explained.

3. Afterwards, in chapter 4, the core idea of complex amplitude modulation is presented as well as the variety of approaches that use this method. Special attention is devoted to the approximation proposed by Arrizon et al, which is the one implemented in this work.

4. In chapter 5 the experimental setup used to develop a novel technique that allows LG-vector beams generation using a SLM in an on-axis configuration is detailed. In this chapter the calculations needed to generate the holograms and to perform the polarization reconstruction are explained.

5. Chapter 6 show the results obtained: representative examples of the generated LG vector beams are provided, together with a characterization of their state of polarization and a quantitative analysis of their purity and stability.

6. Finally, on chapter 7 the main conclusions are highlighted together with the most relevant information concerning the technique implemented. Some ideas about possible improvements are suggested.

Chapter 2

Vector beams

On this chapter the main concepts related with vector beams are shown. First of all, the wave equation is presented; afterwards the approximations needed to deduce the paraxial Helmholtz equation are introduced and the solution in cylindrical coordinates is deduced. The deduction is followed by a description of scalar and vector modes considering the DoFs associated with the spatial form and polarization. Next, some of the generation techniques are summarized. Finally the Stokes polarimetry formalism, which is the base for the characterization of vector beams, is explained.

Once assumed that a feasible description of light is as an electromagnetic wave, it is possible to demonstrate with the help of Maxwell's equations that light is in fact described as a wave function that satisfies the second-order differential equation known as *wave equation*, which involves the reduced speed of light (the rate between the speed of light in free space and the refractive index of the medium by which it is traveling) $c = \frac{c_0}{n}; n \geq 1$. Let us consider the wave equation given by:

$$\nabla^2 \mathbf{E}(\mathbf{r}, t) - \frac{1}{c^2} \frac{\partial^2 \mathbf{E}(\mathbf{r}, t)}{\partial t^2} = 0, \tag{2.1}$$

∇^2 corresponds to the Laplacian operator and is defined in cartesian coordinates by $\nabla^2 = \frac{\partial^2}{\partial x^2} + \frac{\partial^2}{\partial y^2} + \frac{\partial^2}{\partial z^2}$. Any function satisfying this equation, represents a possible optical field. Notice that only the real part of such function has a physical meaning.

By assuming that the complex wave function satisfying equation 2.1 may be expressed as:

$$\mathbf{E}(\mathbf{r}, t) = \mathbf{E}(\mathbf{r}) \exp\left[i(\mathbf{k} \cdot \mathbf{r} - 2\pi\nu t)\right], \tag{2.2}$$

and after substitution of 2.2 in 2.1, one gets the Helmholtz equation [22]:

$$(\nabla^2 + k^2)\mathbf{E}(\mathbf{r}) = 0, \tag{2.3}$$

where $k = \omega/c$ is the wavenumber and is the magnitude of the wave vector $\mathbf{k} = k_x\hat{\mathbf{x}} + k_y\hat{\mathbf{y}} + k_z\hat{\mathbf{z}}$. For a wave traveling along the z direction, the transverse Laplacian, defined as $\nabla_T^2 = \frac{\partial^2}{\partial x^2} + \frac{\partial^2}{\partial y^2}$, is introduced. Therefore $\nabla^2 = \nabla_T^2 + \frac{\partial^2}{\partial z^2}$ and the Helmholtz equation may be written as:

$$\left(\nabla_T^2 + \frac{\partial^2}{\partial z^2} + k^2\right)\mathbf{E}(\mathbf{r}) = 0. \tag{2.4}$$

It is known that a field propagating along z is given by:

$$\tilde{\mathbf{E}}(\mathbf{r}) = \mathbf{E}(\mathbf{r}) \exp(-ikz). \tag{2.5}$$

Substitution of 2.5 in 2.4 gives:

$$\left(\nabla_T^2 + \frac{\partial^2}{\partial z^2} - 2ik\frac{\partial}{\partial z}\right)\mathbf{E}(\mathbf{r}) = 0. \tag{2.6}$$

If the field is varying slowly along the propagation direction compared with the wavelength, that is if $\Delta\mathbf{E}(\mathbf{r}) \ll \mathbf{E}(\mathbf{r})$ for $\Delta z = \lambda$, then the factor $\frac{\partial^2\mathbf{E}(\mathbf{r})}{\partial z^2} \ll k\frac{\partial\mathbf{E}(\mathbf{r})}{\partial z}$ and also $\frac{\partial^2\mathbf{E}(\mathbf{r})}{\partial z^2} \ll k\nabla_T^2\mathbf{E}(\mathbf{r})$ therefore it may be neglected and the previous equation may be reduced to the paraxial Helmholtz equation (PHE):

$$\left(\nabla_T^2 - 2ik\frac{\partial}{\partial z}\right)\mathbf{E}(\mathbf{r}) = 0. \tag{2.7}$$

The simplest solutions for these equations are the well known plane and spherical waves, nevertheless one of the most important solutions for this equation is the Gaussian function, which has unique characteristics, such as: its power is mainly located within a small cylinder surrounding the beam axis, the wavefronts are approximately planar near the beam waist and nearly spherical far from it. Also the emission of many types of lasers take the form of a Gaussian beam. More general families of optical solutions include the Hermite-Gauss for cartesian coordinates, the Ince- and Mathieu-Gauss for elliptical coordinates, and the Laguerre-Gauss for cylindrical coordinates.

2.1 Laguerre-Gauss modes

A given set of solutions for the PHE is often referred as *beam mode*. Those solutions depend on several factors such as the boundary conditions and the coordinate system selected to solve the equation. For a given system, once selected the coordinate system and considering the boundary conditions, one commonly obtain a set of several solutions. The set of solutions form a complete orthogonal basis, which implies that all possible electric fields in the system can be expressed in terms of the set [23, 24]. We will next consider the fundamental case of Gaussian modes, followed by the case of Laguerre-Gaussian modes which correspond to the solution of the PHE in cylindrical coordinates.

2.1.1 Gaussian modes

As stated before, Gaussian beams are relevant because they represent the lowest order that a cavity can support. Additionally, these Gaussian beams are not limited to their own family of solutions but also are included in other families of solutions, because of their versatility and prevalence, their study provide valuable insights that contribute significantly to our understanding of the behavior of other types of beams.

To derive the Gaussian modes, a solution of the form [22]

$$U(\mathbf{r}) = \frac{A_0}{r}\exp(-ikr), \tag{2.8}$$

is proposed: a spherical wave. At points that satisfy $\sqrt{x^2+y^2} \ll z$, that is at points far from the origin and close to the z axis it is true that $r = \sqrt{x^2+y^2+z^2}$ can be

expanded in a Taylor series as:

$$r = z\sqrt{1+\theta^2} = z\left(1 - \frac{\theta^2}{2} + \frac{\theta^4}{8} + ...\right); \theta = \frac{x^2+y^2}{z^2}. \tag{2.9}$$

Up to the second order:

$$r \approx z\left(1 + \frac{\theta^2}{2}\right) = z + \frac{x^2+y^2}{2z}. \tag{2.10}$$

By replacing the Taylor expansion of r on equation 2.8, the Fresnel approximation of a spherical wave is obtained:

$$U(\mathbf{r}) = \frac{A_0}{z}\exp(-ikz)\exp\left(-ik\frac{x^2+y^2}{2z}\right). \tag{2.11}$$

This wave may be seen as a plane wave modulated by the factor $(1/z)\exp\left(-ik\frac{x^2+y^2}{2z}\right)$. As can be seen on figure 2.1, points near the origin are spherical and represent a spherical wave front, while for intermediate points one have a paraboidal form, and for points far from the origin, the phase factor approaches to zero and the wave approaches to a planar wave [22].

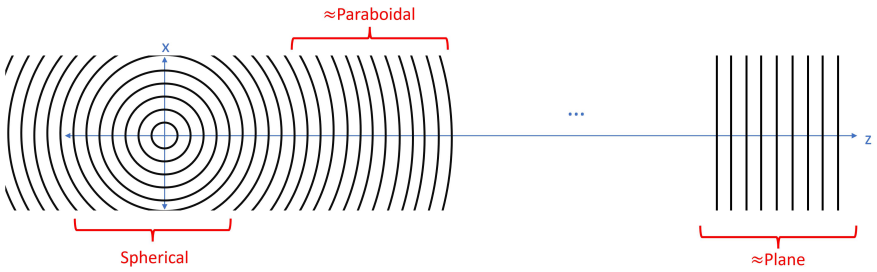

FIGURE 2.1: Graphical representation of Fresnel approximation.

Since a paraboidal wave given by 2.11 is solution of the paraxial Helmholtz equation, one may shift the function an it will also be a solution. Then, by introducing the parameter $q(z) = z + iz_R$, with z_R being the Rayleigh range, equation 2.11 may be expressed as:

$$U(\mathbf{r}) = \frac{A_0}{q(z)}\exp[-ikz]\exp\left[-ik\frac{x^2+y^2}{2q(z)}\right], \tag{2.12}$$

and given the definition for $q(z)$, we may calculate:

$$\frac{1}{q(z)} = \frac{1}{z+iz_R} = \frac{1}{R(z)} - i\frac{\lambda}{\pi\omega^2(z)}, \tag{2.13}$$

for appropriate definitions of $R(z)$ and $\omega(z)$, which will be given later on this chapter. Considering the alternative representation of a complex number in the form $\mathbb{C} = X\exp(-i\xi(z))$ it is possible to rewrite equation 2.13 as:

$$\frac{1}{q(z)} = \frac{\omega_0}{z_R\omega(z)}\exp[\xi(z)]. \tag{2.14}$$

Considering the expressions 2.13 and 2.14 in equation 2.12, one gets the Gaussian beam given by:

$$U(\mathbf{r}) = \frac{A_0\omega_0}{\omega(z)} \exp\left[-\frac{x^2+y^2}{\omega^2(z)}\right] \exp\left[-ikz - ik\frac{x^2+y^2}{2R(z)} + i\xi(z)\right], \tag{2.15}$$

where A_0 is a constant and some important parameters, that can be observed on figure 2.2 have been introduced and are defined as follows:

1. Beam waist ω_0 is the value of the spot size in $z = 0$ and it corresponds to the minimum value of the beam width.
2. Beam width: Refers to a measurement of how the transversal dimension of the beam increases as it propagates:

$$\omega(z) = \omega_0\sqrt{1 + \left(\frac{z}{z_R}\right)^2} \tag{2.16}$$

3. Beam radius: This parameter indicates how much the plane wave-front bends in the plane transverse to propagation.

$$R(z) = z\left[1 + \left(\frac{z}{z_R}\right)^2\right] \tag{2.17}$$

4. Gouy phase: Indicates the measurement of how much the phase of a wave has increased due to its propagation.

$$\xi(z) = \arctan\left(\frac{z_R}{z}\right) \tag{2.18}$$

5. Rayleigh range: Distance from the beam waist, in the direction of propagation, where the beam radius is increased by a factor of $\sqrt{2}$:

$$z_R = \frac{\pi\omega_0^2}{\lambda} \tag{2.19}$$

2.1.2 Laguerre-Gauss scalar modes

Scalar modes are solutions to the PHE [25] and their main feature is that they have spatially homogeneous states of polarization in the transverse plane perpendicular to the direction of propagation, this means that for these beams, the trajectory of oscillation for the electric field remains unaffected, regardless of the position of the observation points within the cross-sectional area of the beam [26]; experimentally one finds that when passing it through a linear polariser, a pattern that changes only in intensity but not in distribution as the polariser rotates, is found.

The Laguerre-Gaussian scalar modes are obtained by considering cylindrical coordinates (ρ, ϕ, z), in which the Laplacian operator is defined as:

$$\nabla^2 = \frac{1}{\rho}\frac{\partial}{\partial\rho}\left(\rho\frac{\partial}{\rho}\right) + \frac{1}{\rho^2}\frac{\partial^2}{\partial\phi^2} + \frac{\partial^2}{\partial z^2}. \tag{2.20}$$

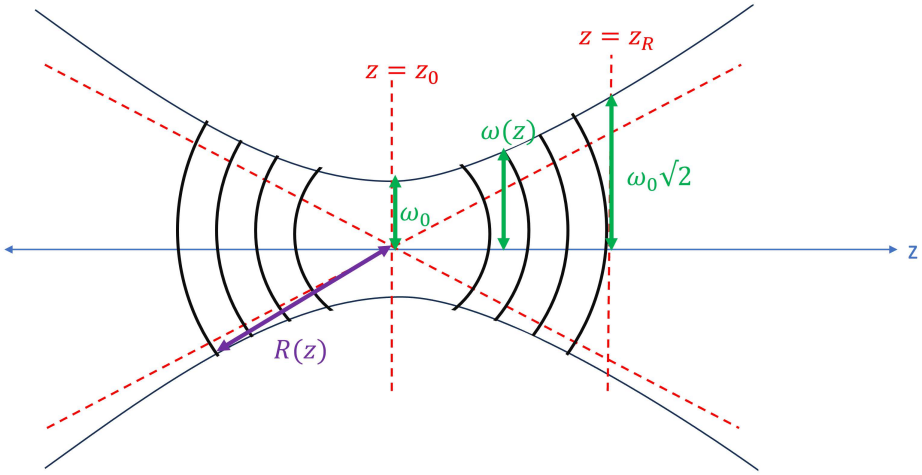

FIGURE 2.2: Graphical representation of the main parameters that describe a Gaussian beam.

Therefore the paraxial Helmholtz equation changes to:

$$\left[\frac{1}{\rho}\frac{\partial}{\partial\rho}\left(\rho\frac{\partial}{\rho}\right)+\frac{1}{\rho^2}\frac{\partial^2}{\partial\phi^2}-2ik\frac{\partial}{\partial z}\right]U(\rho,\phi,z)=0. \tag{2.21}$$

It is possible to show that 2.21 takes the form of the standard differential equation for the Laguerre polynomials, which has the Laguerre polynomials LG_p^l, with radial index p and axial index l, as solutions and are determined by [22, 23, 27]:

$$\begin{aligned} LG_p^l(\rho,\phi,z) &= \frac{\omega_0}{\omega(z)}\left[\frac{\rho}{\omega(z)}\right]^l L_p^l\left(\frac{2\rho^2}{\omega^2(z)}\right)\exp\left(\frac{-\rho^2}{\omega^2(z)}\right) \\ &\quad\times\exp\left[-ikz-ik\frac{\rho^2}{2R(z)}-il\phi+i(l+2p+1)\xi(z)\right]. \end{aligned} \tag{2.22}$$

Where L_p^l are the Laguerre polynomials; $l \in \mathbb{Z}$ is also known as the topological charge; $p \in \mathbb{N}$ is associated to the generation of $(p+1)$ intensity rings along the radial direction; and ω_0, $\omega(z)$, $R(z)$, $\xi(z)$ have the same definitions as for the Gaussian modes, as described above. The function given by 2.22 is a solution for 2.7 and is the mathematical representation of the Laguerre-Gauss modes, which form a complete set of solutions [22]. Note that the lowest order LG beam, that is for $l = p = 0$, corresponds to the Gaussian beam.

The Laguerre-Gaussian modes have been widely studied [28, 29] due to its properties (its circular symmetry, the quantized OAM of photons, and self-similar propagation, among others) and potential applications, mainly in optical trapping [30] and as a valuable tool for manipulating cold atoms [31]. These modes have doughnut-like transverse intensity profiles [32] with bright rings whose radii and OAM contents increase with l , they carry a well defined orbital angular momentum equal to $\hbar l$ per photon [33]. On figure 2.3 a numerical simulation of LG_0^1 scalar modes is shown: In all cases the transverse plane perpendicular to the propagation is shown together with the ellipses and lines indicating its polarization state along the whole profile, nevertheless each beam is different since each beam has a particular polarization state as indicated on the caption of the figure.

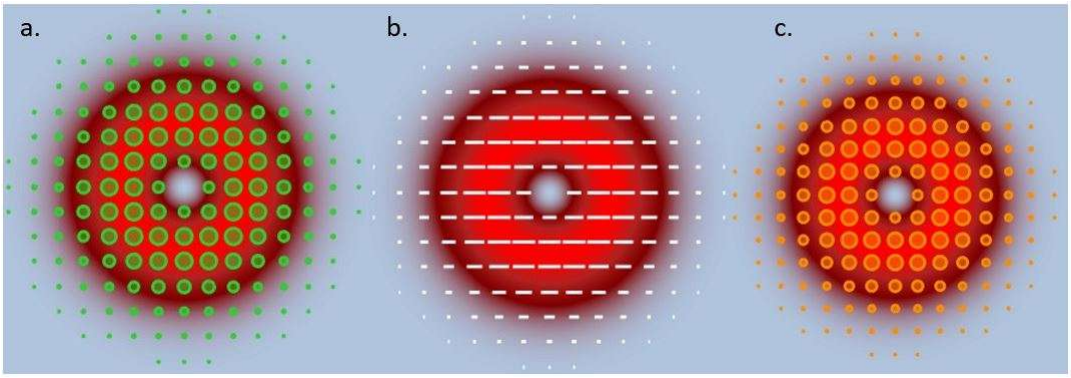

FIGURE 2.3: Numerical simulation of the polarization distribution for three different scalar beams. a) circular-left handed polarization; b) linear polarization; c) circular right-handed polarization.

2.1.3 Laguerre-Gauss vector modes

Any superposition of solutions to the PHE is also a solution of it. If the superposition of two scalar modes that are orthogonal and which have orthogonal polarization states is considered, then a vector beam is obtained. Vector beams are fully polarized but, contrary to the scalar beams, they manifest inhomogeneous distribution of polarization along the plane transverse to its propagation [7]. This is equivalent to state that "the spatial mode and polarisation are non-separable and should be described as such" [6]. The inhomogeneities in polarization may be observed by placing a linear polariser between the intensity profile and the detector, then a different distribution will be seen depending on the orientation of the polariser. Vector beams, and particularly Laguerre-Gauss vector modes, are widely used in applications that include STED microscopy [34].

Vector beams are mathematically described as [35]:

$$\mathbf{U}(\mathbf{r}) = u_1(\mathbf{r}) \cos\theta \hat{R} + u_2(\mathbf{r}) \sin\theta e^{i\alpha} \hat{L}, \tag{2.23}$$

where $u_1(\mathbf{r})$ and $u_2(\mathbf{r})$ are two orthogonal spatial modes; $\cos\theta$ and $\sin\theta$ with $\theta \in [0, \pi/2]$ are weighting factors that allow the transition between a purely scalar mode (when $\alpha = 0, \pi/2$) to a purely vector mode (when $\alpha = \pi/4$) [6]; $\hat{R}$ and $\hat{L}$ are unitary polarization vectors for right and left circular polarization, respectively; finally, $\alpha \in [0, \pi]$ is a phase difference between both fields, known as the intermodal phase.

A schematic representation of three different vector beams may be seen on figure 2.4, where the green ellipses correspond to circular-left handed polarization; the white lines to linear polarization and the orange ellipses to circular right-handed polarization. Notice that b) has only linear polarization but the direction at each point changes; whereas a) and c) have not only different orientation of the polarization at each point but also the type of polarization changes.

It is worth mentioning a few words about the intermodal phase because it determines the temporal stability of the beam: variations of α permit the transition between different vector beams, for example if $\alpha = 0$ then a radially polarized beam is obtained, while for $\alpha = \pi$, one have an azimuthal polarized beam; and values in between give place to spirally polarized beams [35]. Theoretically the intermodal phase is a constant value, but for some cases of the experimental generation of vector beams, fluctuations due to differences in the optical path of the scalar beams that are

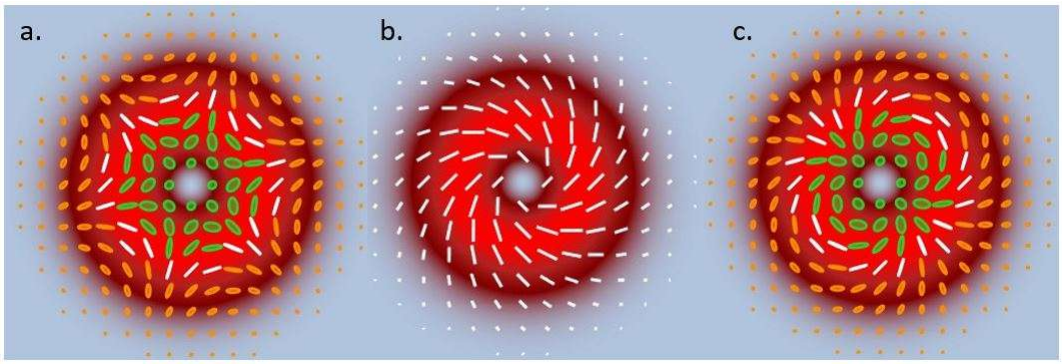

FIGURE 2.4: Numerical simulation of the polarization distribution for three different vector beams: a) web-like polarized beam; b) spirally polarized beam; c) spider-like polarized beam.

superimposed to form the vector beam introduce an additional intermodal phase that is not constant.As a result of the later, the vector beams generated are not stable and manifest random oscillations between beams with several polarization states: if the intermodal phase changes, the beam is not stable.

For the case of Laguerre-Gauss vector modes, equation 2.23 takes the form [36]:

$$\mathbf{U}(\mathbf{r}) = \frac{\sqrt{2}}{2}\left[LG_{p_1}^{l_1}(r)\cos\theta\hat{R} + LG_{p_2}^{l_2}(r)\sin\theta e^{i\alpha}\hat{L}\right], \tag{2.24}$$

the modes generated and reported in this work are limited, due to the technical implementation, for cases where $l_1 = -l_2$ and $p_1 = p_2$.

2.2 Vector beam generation techniques

Because of the versatility of its potential applications in areas such as optical trapping and manipulation [11], quantum communications [14], microscopy [34], among others; and thanks to the technological advances, the generation and characterization of vector beams has been a topic with high activity in the last years (see for example [16, 37, 38] and references therein). Concerning generation techniques, it is possible to classify them in two categories: geometric [39, 40] and dynamic phase modulation [41, 42].

The geometric phase techniques "involve a direct conversion of optical angular momentum from the spin to the orbital form" [43], and refer to those techniques that are based on the use of "spatially patterned retarders where the orientation of the principal axis has a spatial variation" [37]. The canonical example of geometric phase optical elements is the q-plate, invented in 2006 and characterized by the topological charge of the central singularity [44]; and its more generalized alternative, the J-plate (introduced in 2017 as an alternative to overcome the drawbacks of the q-plates, and based on the use of nano-structures [45]).

In spite of such techniques being highly efficient and straightforward techniques that do not demand for complicated optical arrangements, there are some disadvantages when using these elements, being of great relevance the fact that they have a limited performance and are useful only for the generation of a particular optical field with specific characteristics [37, 38].

Dynamic phase modulation techniques imply a change in the optical path and include those techniques that rely on the use of diffractive elements, lithographically produced sub-wavelength polarization gratings, or interferometers to split a beam in two beams that propagate through different paths, which allows the independent manipulation of the polarization, amplitude and phase of each beam before their superposition [46]. Among interferometric approaches SLMs provide "a more flexible way to generate the desired fields" [24, 47] and has been pointed out as one of the most commonly used techniques because of the advantages it offers, specially the rapid creation of nearly any vector beam and the display of unconventional, intricate patters in spatial and polarization distributions. More details about some generation techniques based on the use of SLMs is provided on chapter 3.

2.3 Characterization of vector beams

The polarization of a beam is a fundamental quantity that arises from and illustrates the vector nature of light [48]. Polarization determines the direction in which the electric field oscillates as it propagates and evidences its variation in time. In this section, the general formalism to describe and represent the state of polarization of light, which allows for the characterization of vector beams, is provided.

For a given optical field propagating along the z-direction in free space, its state of polarization along the transverse plane can be represented by:

$$\begin{aligned} E_x &= E_{0x}\cos(\tau + \delta_x)\hat{i} \\ E_y &= E_{0y}\cos(\tau + \delta_y)\hat{j}, \end{aligned} \tag{2.25}$$

where E_{0x} and E_{0y} are the $x-$ and $y-$ amplitude components of the field; the term $\delta = \delta_y - \delta_x$ determines the phase delay between both components; $\tau = \omega t - kz$ is called space-time propagator, with ω being the frequency of a light beam assumed to be monochromatic.

By eliminating the propagator in equations 2.25 and the appropriate algebra, it is possible to arrive to an expression called the polarization ellipse, which describes a behavior that "is spoken of as optical polarization" [49]:

$$\left(\frac{E_x}{E_{0x}}\right)^2 + \left(\frac{E_y}{E_{0y}}\right)^2 - 2\frac{E_x E_y}{E_{0x}E_{0y}}\cos\delta = \sin\delta^2. \tag{2.26}$$

For special considerations, equation 2.26 leads to forms that are known as degenerate states (or scalar modes) and which correspond to: linear horizontally or vertically polarized light, for the cases when $E_{0y} = 0$ or $E_{0x} = 0$, respectively; linear $\pm 45°$ polarized light if $E_y = \pm E_x$ and $\delta = 0, \pi$; finally, for $E_{0x} = E_{0y}$ one have right circularly polarized light if $\delta = \pi/2$ and left circular polarized light if $\delta = 3\pi/2$.

Another important consideration to be made is how the parameters E_{0x}, E_{0y} and δ in equation 2.26 can be related to the parameters that conventionally represent an ellipse: the angle of rotation (which is measured relative to the $x-$axis), $\psi \in [0, \pi]$; and the ellipticity angle, $\chi \in [-\pi/4, \pi/4]$. By geometrical considerations, in [50] the deduction of the following expressions for both parameters is detailed:

$$\tan 2\psi = \frac{2E_{0x}E_{0y}}{E_{0x}^2 - E_{0y}^2}\cos\delta,$$

$$\tan 2\chi = \frac{2E_{0x}E_{0y}}{E_{0x}^2 + E_{0y}^2} \sin\delta. \tag{2.27}$$

It is important to recall that by determining those quantities, the polarization of a beam may be fully described. As will be shown in the next section, with the aid of Stokes parameters, that can be expressed in terms of intensities, which are measurable quantities. In figure 2.5 a geometrical representation of the polarization ellipse is shown.

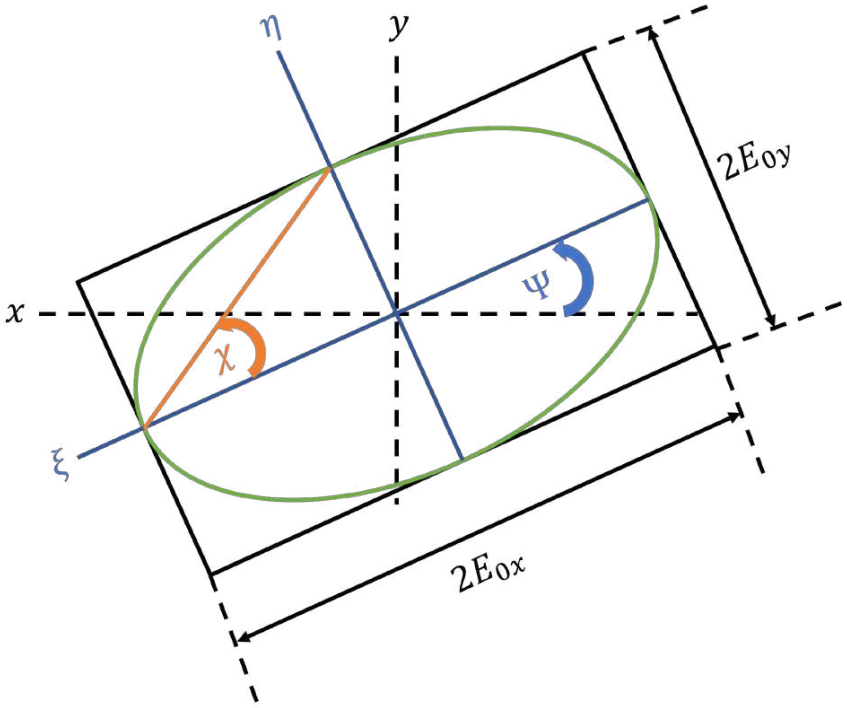

FIGURE 2.5: Polarization ellipse, where Ψ is the angle of rotation, χ is the ellipticity angle, E_{0x} is the semi-major axis and E_{0y} is the semi-minor axis.

2.3.1 Stokes polarimetry

Notwithstanding its usefulness to represent several states of polarization in a single equation, the polarization ellipse does not result practical for several reasons, among them: the impossibility to observe it directly due to the quick variations it has in time, and the fact that it can describe only completely polarized light and not unpolarized or partially polarized light. A more useful and versatile approximation, given in terms of observable quantities, was proposed for the first time around 1852 by Sir George Gabriel Stokes: the Stokes polarization parameters, which can be directly related to the polarization ellipse and its orientation [51], are determined by intensity measurements as:

$$\begin{aligned} S_0 &= I_0 = E_{0x}^2 + E_{0y}^2, \\ S_1 &= I_H - I_V = E_{0x}^2 - E_{0y}^2, \\ S_2 &= I_D - I_A = 2E_{0x}E_{0y}\cos\delta, \\ S_3 &= I_R - I_L = 2E_{0x}E_{0y}\sin\delta. \end{aligned} \tag{2.28}$$

In equation 2.28 I_0 stands for the total intensity of the given field and it satisfies:

$$I_0 = I_H + I_V = I_D + I_A = I_R + I_L. \tag{2.29}$$

The intensities I_H, I_V, I_D, I_A, I_R and I_L are the measured intensities when the beam is passed through a linear horizontal polarizer (LHP), a linear vertical polarizer (LVP), a linear $+45^\circ$ polarizer, a linear -45° polarizer, a right circular polarizer, and left-circular polarizer, respectively [50]. Each Stokes parameter has a physical meaning: S_0 indicates the total intensity of the optical field, while S_1, S_2 and S_3 refer to the tendency of the beam (that is, how close is the beam's polarization state) to have linear horizontal or vertical polarization, $+45^\circ$ (diagonal) or -45° (anti-diagonal), and right or left circular polarization, respectively.

Even more, the degree of polarization may be defined in terms of Stokes parameters as:

$$P = \frac{\sqrt{S_1^2 + S_2^2 + S_3^2}}{S_0}, \tag{2.30}$$

and this quantity provides the required information to determine if light is totally polarized ($P = 1$), partially polarized ($0 < P < 1$) or unpolarized ($P = 0$). For the cases that will be produced and analyzed in this work, we are restricted to a laser beam, which is closely approximated to a monochromatic totally polarized field.

Using 2.28 in 2.27 it is possible to express the ellipse parameters in terms of Stokes parameters as:

$$\begin{aligned} \tan 2\psi &= \frac{S_2}{S_1}, \\ \tan 2\chi &= \frac{S_3}{S_0}. \end{aligned} \tag{2.31}$$

And considering 2.29, Stokes parameters may be written as:

$$\begin{aligned} S_0 &= I_R + I_L, \\ S_1 &= 2I_H - S_0, \\ S_2 &= 2I_D - S_0, \\ S_1 &= 2I_R - S_0, \end{aligned} \tag{2.32}$$

it can be clearly seen that in order to determine the state of polarization of a beam, it is sufficient to perform the four intensity measurements for I_R, I_L, I_H and I_D. The experimental details about how these measurements are performed in the laboratory are provided in chapter 5.

2.3.2 Purity analysis

The vector purity is a measure of the degree to which a beam is non-separable in polarization and spatial degree of freedom [52]. Traditionally, the experimental differentiation between vector and scalar beams is performed only by a qualitative approach: a linear polarizer is placed after the beam and then it is rotated, if a change in the intensity distribution is seen, then a vector mode is confirmed, otherwise the mode is scalar [6]. Nevertheless, as stated previously, an important characteristic of vector beams is that their spatial and polarization DoFs are non-separable.

If 2.23 is written using Dirac notation from quantum mechanics, one obtains the expression [53]:

$$|\Psi_l\rangle = \cos\theta\,|l\rangle\,|\hat{R}\rangle + \sin\theta e^{-i\alpha}\,|-l\rangle\,|\hat{L}\rangle\,, \tag{2.33}$$

which resembles the expression of a entangled two-particle quantum system. Besides that, as stated by Nape and collaborators [18], since "non-separability is not unique to quantum mechanics, many of the tools for measuring this must be applicable to vector beams too". For example it was shown by McLaren et al in 2015 [18] that a Bell-like inequality measurement [54] indicates if a given field is scalar or vector; and concurrence measurement [55] provides information about the degree to which the field is vectorial, assigning a number between 0, which corresponds to a fully scalar field, and 1 in the case of fully vector field (values in between refer to "non pure" states; that is states in which one of the components is weighted higher than the other).

A year later, in 2016, Ndagano et al [19] emphasise that in spite of the agreement about the fact that the purity of scalar beams can be measured by the beam quality factor M^2, there is a lack of a quantitative measurement to determine the "purity" of vector modes and clearly differentiate them from scalar modes; further they introduce the vector quality factor (VQF) in terms of the concurrence, as expressed by McLaren et al. In their work, Ndagano et al show experimentally that the values taken by the VQF goes from 0 to 1 and that it does not depend on the type of vector beam or the basis used to perform the measurements. The VQF is expressed as [19]:

$$VQF = Re[C] = Re\left[\left(1 - \sum_{i=1}^{3}\langle\sigma_i\rangle^2\right)^{1/2}\right], \tag{2.34}$$

where $\langle\sigma_i\rangle$ are the expectation values of the Pauli operators, representing a set of normalized intensity measurements, which as detailed in [19] "resemble the Stokes parameters used in recovering the polarization distribution, but are fundamentally different: they do not represent a series of polarization measurements but rather a series of holographic measurements of the spatial field, and result in a measure of the degree of non-separability of vector beams", though the quantification of vector beam purity is, in principle, difficult to implement because it involves spatial projective measurements. Luckily, in 2019 an alternate form to measure the concurrence C, thus the VQF directly from Stokes parameters is proposed [20]:

$$C = \sqrt{1 - \frac{\mathbb{S}_1^2}{\mathbb{S}_0^2} - \frac{\mathbb{S}_2^2}{\mathbb{S}_0^2} - \frac{\mathbb{S}_3^2}{\mathbb{S}_0^2}}, \tag{2.35}$$

where $\mathbb{S}_i$ corresponds to the values of the Stokes parameters S_i integrated over the whole transverse profile of the beam:

$$\mathbb{S}_i = \int\int_{-\infty}^{\infty} S_i dA; i = 0, 1, 2, 3. \tag{2.36}$$

This approach is the one used on this work to determine the purity of the generated beams.

2.3.3 Stability analysis

Temporal stability of a vector beam can be measured directly from the variation of ellipticity and orientation of the polarization states along the plane perpendicular to beam propagation. Even more, since instability of vector modes is a completely random process, if the beam is unstable and its Stokes parameters, given by equation 2.32, are measured for two different times, regardless of the time interval in which the measurements are performed, the values for ellipticity and orientation of the polarization will be different. Therefore, in order to quantify the stability of the generated vector modes it is sufficient to consider the value of these quantities as a function of time.

To do so, the same methodology followed by Perez-Garcia and collaborators in [21] will be considered. On their work, to asses the performance of the implemented setup, the theoretical and experimental values of the orientation and flattening (a measure of the shape of polarization where $f = 0$ corresponds to a circularly polarized state and $f = 1$ to a linearly polarized state) were compared by calculating the root mean squared error (RMSE) of both parameters for each polarization ellipse across the transverse plane. The orientation angle and flattening are given as:

$$\begin{aligned} \alpha &= \frac{1}{2}\arctan\left(\frac{S_2}{S_1}\right) \\ f &= \frac{A-B}{A} \end{aligned} \tag{2.37}$$

where S_i corresponds to the Stokes parameters and the terms A and B are the semi-major and semi-minor axis, respectively; and can be calculated using the Stokes parameters:

$$\begin{aligned} A &= \sqrt{\frac{1}{2}\left(S_0 + \sqrt{S_1^2 + S_2^2}\right)} \\ B &= \sqrt{\frac{1}{2}\left(S_0 - \sqrt{S_1^2 + S_2^2}\right)} \end{aligned} \tag{2.38}$$

However, an important difference between the comparison made in [21] and the one that was performed in this project is that instead of comparing the theoretical and experimental values, three different measurements of intensity for each beam were made and the root mean squared error was computed considering the measurement at a time $t = t_1$ as the expected value in contrast to the values obtained for $t = t_2$ and $t = t_3$.

Chapter 3

Spatial light modulators (SLMs)

As stated on the previous chapter, as the interest in using tailored vector beams increases, so does the amount of techniques that facilitates its generation and characterization. Among those techniques we can find different approaches such as those using liquid crystal wave-plates, glass cones, interferometric arrays, and digital holography. The latter is one of the most flexible and versatile and allows the generation of a huge amount of different fields with particular phase, intensity and polarisation distribution. In this chapter we explain in more detail how the Spatial Light Modulators are used to modulate the properties of light; in the same way, basic information about the SLMs and its working principle (liquid crystals properties) is provided. Finally, a brief comparison between SLMs and DMDs is presented.

3.1 Liquid crystals

Solid, liquid, and gas are the most evident states (or phases) in which matter may be found, the differences between these phases rely mainly on the level of positional and orientational order that the molecules posses [56]; nevertheless there are intermediate states (also known as mesomorphic phases [57]) that show a behavior in between those states (in figure 3.1 a diagram representing the main states of matter as well as the possible transitions between states is shown). In general, the solid, liquid and gas phases are stable for a certain range of temperature, if the temperature is changed, the amount of order among the molecules also changes and so does the phase [58]. One of such intermediate phases is a phase discovered in 1888: liquid crystals (LCs), which represent "a fascinating state of matter that combines order and mobility at multiple hierarchical levels" [59]. LCs are arrangements of molecules with some specific characteristics: elongated in shape with some rigidity in its central region and flexible ends, rod-like (or disk-like), organic, easy to polarize.

LCs posses some typical properties of liquids as well as some properties of solids: for example the property of flowing like a liquid (which means no long-range order in at least one of the directions); formation and fusion of droplets; birefringence by the anisotropy of optical, electrical and magnetic properties, which means that their properties depend on the direction in which they are viewed (and implies that there exists long-range order in at least one of the directions) [57, 60, 61], interestingly the refraction index can be controlled electrically thanks to the anisotropies (optical and dielectric) on LCs [62]. In spite of being an intermediate state, a means of measuring the orientational order in a liquid crystal is called order parameter, its typical values range $0.3 - 0.9$ [58], where a value of 1 would mean perfect orientational order (solid-like) and a value of 0 corresponds to no orientational order (liquid-like); this value

decreases as temperature is increased, this together with the latent heat of the phase transition between solid an liquid crystal compared with that of liquid crystal to liquid, may be useful to evidence if liquid crystals are more similar to liquids than they are to solids or vice versa.

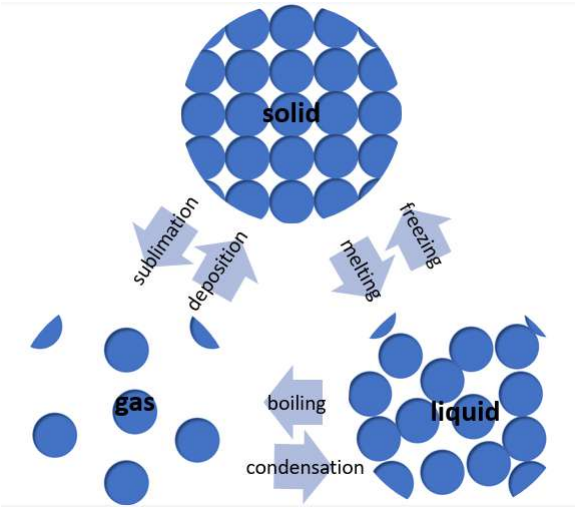

FIGURE 3.1: Diagram representing the three main states of matter: solid, liquid and gas. Intermediate phases may be found in the transition (blue arrows) from one into another. When going through melting, some solids may reach a liquid-crystal state before the liquid state.

Other characteristics of LCs include a change in their visual appearance when transitioning from one phase to another; the property to eliminate defects by self-healing; the existence of either intrinsically permanent or induced electric dipole; they work under low voltage and low power and that they can often operate correctly in the presence of sunlight; the configuration (arrangement) of liquid crystals' structure is associated with the ability to easily respond under external stimuli and change their configuration [57, 61], for example the photorefractive effect that is used to produce re-writable and dynamic holographic images; and the fact that when applying an external electric or magnetic field, molecules tend to arrange in a direction parallel or perpendicular to the applied field, then the structure of the liquid crystal changes together with the optical transmission properties [60, 63].

There are several types of LCs and their formation depends on several factors such as the constituent molecules, temperature, concentration and solvents; although many of their characteristics are shared, depending on the arrangement mechanism LCs may be considered lyotropic (formed by colloidal solutions, sensitive to concentration and temperature) or thermotopic (created by heating crystalline structures, temperature-dependent) [59]. In turn, the latter are subdivided based on the molecular arrangement and symmetry (as can be seen on figure) in: nematics (molecules tend to be parallel to some common axis and it can occur only in systems where there is no distinction between right and left, have a strong dipole moment and high refractive index); cholesterics (periodic orientation along the z-direction, helix-like configuration); smectics (layered structures with a well defined inter-layer spacing, more ordered than nematics); and columnar phases (discotic molecular structures stacked in columns and organized in various shapes) [57, 59, 64, 65].

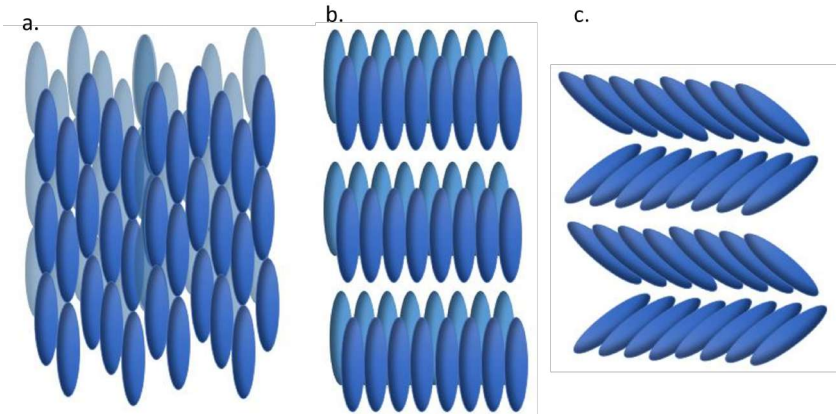

FIGURE 3.2: Schematic representation of the molecular arrangement in different types of LCs: a) nematic; b) smectics; and c) cholesterics.

LCs are ubiquitous in technological applications [66, 67, 68] as detection of hot points in microcircuits, localization of tumors in humans, conversion of display screens, real-time holography, diffractive optics, optical imaging, plasmonics, solar cells, photonic crystals, photovoltaics as well as nanophotonics. It is important to note that when thinking for applications in specific devices, "liquid crystals need to be forced and adequately aligned. Therefore, samples are formed between a pair of surface treated glass plates with about few microns distance" [61]. Fortunately, concerning the current developments in synthesis and characterization, it is possible to generate devices with specific electro-optical effects, actuation, chromism, sensing, templating and other interesting features, particularly those including display devices [59, 61].

Specifically, the liquid crystal on silicon (LCOS) devices are a technology based on both the properties of liquid crystals and the advantages of high-performance silicon complementary metal oxide semiconductor (CMOS): LCOS devices can work in transmission or reflection and may be used to alter the polarization and/or phase of an incident beam [65]. A relevant constituent of these devises are the pixels: aluminum mirrors deposited on a silicon backplane substrate which contains also the electronic circuitry, because of their sophisticated configuration, it is possible to control the phase retardation of the incident field on each pixel across the device by changing the applied voltage. LCOS with LCs in the nematic phase have slower response times and are the most widely used due to ease manipulation. The spatial light modulators (SLMs) are an example of this technology.

Already in 1992, when applications of LC were mainly focused on display technologies serving as a fundamental bridge allowing the interaction of people with technology [56], the great influence of LC-based technology was envisioned as the prevailing method for transmitting information within modern technological society [56] which was expected to play even a bigger role in the future. The high potential of LCs and their intended economical perspectives together with the fact that there are still challenges to overcome (such as residual DC charges, ionic impurities that may lead to disruptions on the display application), make research on this field very appealing and active [59].

3.2 Characteristics of SLMs

Spatial light modulators are quasi-planar opto-electronic and programmable devices arranged in a pixelated manner that allow the manipulation of some properties (amplitude, phase, and polarization) of light. The use of SLMs as "diffractive optical elements in optical systems to facilitate flexible control of light beams" [69] is extensively spread, their implementation in many fields such as imaging, digital holography, optical switching, micro-structure fabrication, and optical vortex generation is widely generalized [70].

Although at the beginning SLMs consisted of "complex setups that required an expert to use them" [71], the extended use in several fields, including not only research and implementations but also the pedagogical realm, permitted their incorporation as a well-established optical technology capable to work in a plug-and-play manner that a non-expert can use with only a little knowledge [72]. In fact, for their usage, no specialized software is required, one only needs to connect it to a computer and then it can be used as a second monitor.

The properties, and thus the physics, of liquid crystals is the principle governing SLMs' behavior. Each pixel on the array allows a local, independent and dynamic control of the optical path of the light passing through it or being reflected off it, that is, SLMs may be implemented upon transmission or reflection [5, 73], the latter is the implementation followed on this work. In order to control each pixel, and consequently the properties of the incident light it is necessary to adjust the voltage applied on each pixel, which will change the orientation of the LC's molecules and, by birefringence, will induce the phase change [6].

In essence, the beam is shaped by the suitable codification of the phase and amplitude into the SLM, that is: by finding the appropriate image and encode it (the computer generated hologram, CGH or digital hologram) it is possible to produce virtually any desired result [5]. In the complex amplitude modulation approach (which is described in detail on the next chapter), a digital hologram pattern, with gray levels in the interval $[0, 255]$ encoding the complex amplitude, is displayed on the SLM, allowing the transformation of the incoming beam for the creation of an output beam with the desired structure; each gray level corresponds to a pixel voltage and to a specific orientation of the liquid crystal's molecules and is associated to a discrete increment of the phase from 0 to 2π, albeit the obtained response may vary from the ideal response due to external factors such as defects during manufacturing, the non-linear effects produced on the LC, possible anomalies within the surface, and the conditions of operation (incident angle, power supply, frame rate, etc.), among others [74]. Hence calibration before first use is suggested for optimal utilization.

In general, after light reaches the SLM, it will be diffracted as effect of the grating formed by the pixel array but there will always be an undesired effect: a portion of light (that goes from 5% to 20%) that is undiffracted and consequently does not interact with the hologram, if it is not separated from the diffracted light, the two components may interfere. To overcome this effect, a blazed grating is codified into the SLM together with the desired phase-shift, it will act acts as a linear phase ramp, having the effect of moving the desired beam away from the undiffracted beam (located on the zeroth order). As a matter of fact, for certain cases, when working in the first diffraction order, calibration of the SLM is a secondary aspect, as concluded by Spangenberg and collaborators in their work, the calibration of the SLM

may not even be necessary [69] since it will have almost the same response for all wavelengths with only minor effects in the amplitude.

SLMs may be classified depending on how they are being used, which is the optical parameter they modulate, and the type of driving signal. The most common type of SLM is the electro-optical liquid crystal display, which includes transparent liquid crystal displays for the transmissive types and liquid crystal on Silicon for the reflective ones. Regarding the molecular alignment, which impacts on how the beam is manipulated, there are three possible configurations: parallel aligned nematic (PAN), vertically aligned nematic (VAN), and twisted nematic (TN). In the latter the orientation of the molecules in the bottom and top layers are rotated by a fixed angle; while in the two former all layers are parallel to each other [74].

Because the modulation allowed by the majority of commercial SLMs is restricted to either phase- or amplitude-only (or mostly) modulation of light, several approaches using only one SLM to control more than one DoF simultaneously and independently have been proposed but there are still challenges to overcome. Already in 2016 the relevance of SLMs as a tool for creating on-demand arbitrary optical fields was pointed out as well as the approaches using complex amplitude modulation on phase-only SLMs [75].

Figure 3.3 shows a schematic representation of the LCOS-SLM's configuration: A layer of LC molecules is inserted between two transparent alignment films, followed on one side by transparent electrodes, afterwards it is covered with a flat glass substrate; on the other side, at the bottom lies a silicon substrate above which an active matrix circuit, that permits the control of each pixel electrode by the applied voltage; this matrix is connected to the pixelated electrodes (typically made of reflective aluminium mirrors) [5, 74].

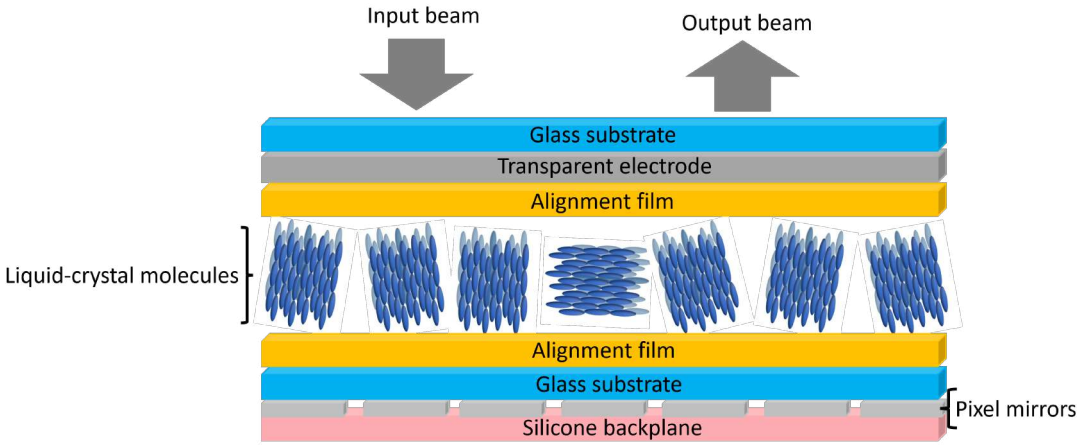

FIGURE 3.3: Configuration of a LCOS-SLM.

An important characteristic of SLMs, generally considered as a drawback, but which results fundamental for the implementation described on this work, is their polarization dependency, which means that SLMs allows the modulation of light under a specific polarization state: typically linear horizontal [38]. Among the advantages, thanks to the superposition principle in optics, it is possible to highlight their ability to allow a multiplexing approach; additional to the fact that SLMs allow encoding arbitrary phase functions, have wide availability, posses technological maturity, and can be reprogrammed [74, 76, 77]; additionally to the possibility of providing

precise, repeatable, and re-configurable optical modulation patterns [78], SLMs also "have the potential to eliminate the undesired artifacts (low resolution, noise, etc.) in holographic applications resulting in dynamic modulation response and high resolution" [74]. Disadvantages of SLMs include the wavelength-dependency of their modulation efficiency, refresh rate ($60Hz$), and high price (though a low cost SLM has been introduced by Huang et al [79]).

Relevant features to fully characterize the SLM perform are: active area (for scientific applications values are usually around $1-2cm^2$; transmittance/reflectance is limited by several factors but mainly by losses in the multiple layers (values ranges from 70% to 90%); spectral acceptance, which for practical uses covers the visible and near infrared (with a bandwidth of $\approx 200nm$; spatial resolution, which is related to pixel density and cross-talk between adjacent pixels (commonly around 40 lines per $/mm$); response time (typical values range $1-100ms$; filling factor, refers to the zones over the SLM's surface that permit an active control of the incident light (slightly above 90% in commercial systems); flicker, which refers to the phase fluctuation because of the electric polarization of the molecules in the liquid crystal (commonly this value corresponds to 0.1π; and damage threshold, which is limited by electrodes and coating materials (around $5W/cm^2$ for continuous radiation and $0.1J/cm^2$ for pulsed femtosecond lasers) [70]. All previous criteria must be considered in order to find the SLM best suited for the targeted application.

Finally it is worth to mention a few words about digital micro-mirror devices (DMDs) which are micro-electronic mechanical systems consisting on a periodical array of micro-mirrors each of which is free to move in two positions known as the "on" and the "off" positions; DMDs work with binary holograms and have emerged as an alternative to the use of SLMs, due to their high modulation rates (up to $30kHz$), wavelength- and polarization-independence and low costs, in diverse areas such as atomic physics, quantum information, novel microscopy, scattering medium, optogenetics, spectroscopy, data storage, simulation of turbulence and particles with rapid motion, and also vector beam generation [80, 81, 82, 83]. Nevertheless, some disadvantages of DMDs include limited modulation depth and low diffraction efficiency [38, 84].

3.3 Light modulation using SLMs

The use of SLMs is only one of many ways (which include the implementation of DMDs, phase plates, cylindrical lens pair, integrated devices, fiber based techniques, etc.) to modulate or produce light with specific characteristics, and the techniques are widely diversified; the central point of those techniques consists on modulate the two-dimensional transverse properties (phase, amplitude, polarization or a combination of them) of an input Gaussian beam either by a single pass, multiple sequential passes, or by the use of two SLMs [16]. In this section, a few out of the many available methods and techniques to generate structured light using SLMs are presented and briefly explained, for most of the cases the applications envisioned by the authors are standed out.

First of all, two approaches that generate the structured beam inside the cavity will be highlighted: On one side is the work of Ngcobo and collaborators [85], who presented in 2013 what they called "a digital laser comprising an electrically addressed reflective phase-only spatial light modulator as an intra-cavity digitally addressed holographic mirror" (see figure 3.4); by the modification of the hologram displayed

on the SLM, the modulation of amplitude-only, phase-only or both may be implemented; in this technique both phase and amplitude are modulated using complex amplitude modulation and a phase-only Hamamatsu LCOS-SLM X110468E series device, which acts as a holographic mirror allowing the generation on-demand of vector modes in real-time (all holograms were designed with standard well-known techniques). Before the generation of arbitrary modes, the performance of the digital laser as a standard stable cavity was verified and it was followed by the successful generation of Hermite–Gaussian, Laguerre–Gaussian, super-Gaussian (flat-top) and Airy beams; limitations on this technique come mainly from the resolution and threshold of the SLM selected while advantages include its accessibility and potential applications in controlling thermal lensing and aberrations in real-time.

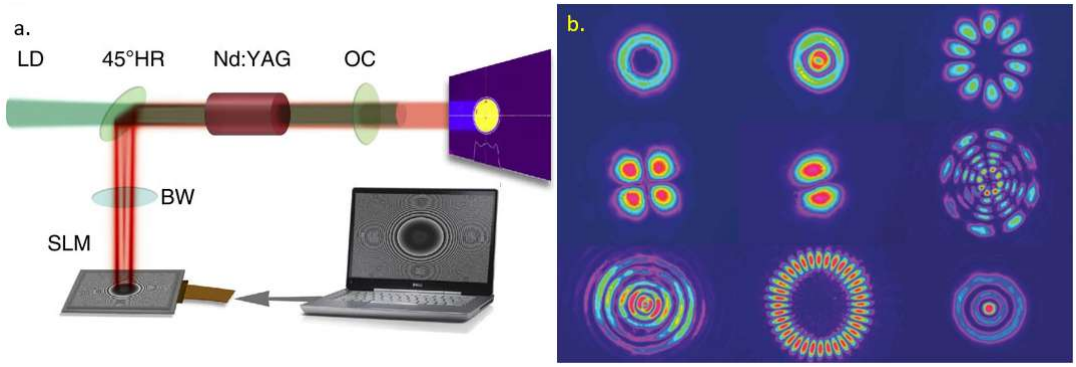

FIGURE 3.4: a) Schematic of the digital laser: A conventional resonator but with a SLM as the back optical element of the cavity, ND:YAG is the gain medium and it is pumped by an external laser diode (LD) source and the output coupler (OC), the SLM is used to display the CGH; and b) example of the Higher-order Laguerre-Gaussian modes created with the digital laser. Taken from [85].

The second approach, following the same line, is the one made by Burger and collaborators in 2015 [86]. They started with a conventional resonator containing two reflective mirrors comprising a stable cavity; through subsequent steps this was replaced by equivalent resonators ending in a configuration comprised by a reflective mirror and a reflective SLM with the adequate hologram displayed on it. Two variations were tried, by modifying the type of liquid crystal used in the SLM (ensuring vertical polarization is essential since SLMs require linear vertically polarized light for optimal operation): one composed by a twisted-nematic liquid crystal, and the other by a parallel-aligned one. With both configurations they found that "intensity distribution pattern in the near-field was the same as that of the far-field, which showed that these laser modes are also free-space modes and invariant on propagation" [86].Their device allows for transverse mode control; they tried with phase-only holograms and also with the complex amplitude modulation technique. The main restrictions of the designed device are imposed by the characteristics of the SLM: resolution and output power (given by the threshold damage).

It is important to recall that when shaping light, it is desirable to have full control of the field (amplitude and phase), and not only one parameter, because this allows the generation of beams with special and controllable properties. In what concerns extra-cavity generation of vector beams using SLMs, to achieve the control of the two polarization components it is necessary to divide the screen into two halves, passing the beam twice through the SLM after a proper polarization transformation, or propose optical arrangements with two SLMs. Methods based on the use of SLMs

require "bulky optical systems but their programmability offers a great flexibility" [76].

In 2000, Davids and collaborators [41] summarized two previously reported techniques: both using a LC-SLM but the first system with the capability of rotating the principal axes of that elliptical polarization state by an arbitrary angle and the other with the capability of generating an arbitrary state of elliptical polarization. They included for the first time a demonstration of the 2-dimensionally codifying capability for controlling the polarization state of a light beam by the use of a parallel-aligned liquid-crystal SLM: with the first technique an arbitrary rotation of the major axis for elliptical light is shown; while the second technique is used to change linearly polarized light to arbitrary elliptically polarized light; the authors highlight the fact that both techniques may be combined to generate a totally arbitrary polarization state. In this work it is outstanded the fact that each pixel of the SLM behaves as a voltage-controlled wave plate, therefore by changing the applied voltage, a phase shift from 0 to $2\pi rad$ (as a function of pixel position) may be induced. The transmitted beam is analyzed finding an unexpected edge-enhancement suggesting applications in image processing and information encryption.

Davis, Valadéz, and Cottrell proposed in 2003 [87] an easy-to-implement-technique (which is an improvement of a previous work of themselves) in which amplitude and phase are encoding (with a linear or quadratic carrier) onto a binary phase-only SLM, by introducing amplitude information through the spatial modification of the diffraction efficiency of a phase-only mask based on the spatial modification of the diffraction efficiency and redirecting the desired light in a specific direction. In this approach light that is not diffracted onto the first order (desired light) is sent to the zeroth order. This technique is said to find applications in optical pattern recognition and image processing.

Neil and collaborators (2002) [88] proposed a method to generate arbitrary complex vector wave fronts that influenced further approaches of several researchers and consists on the implementation of a reconfigurable ferroelectric liquid-crystal SLM (a reconfigurable binary optical element) in a off-axis configuration to control the wave front and which also permits aberration correction. To produce an arbitrary scalar beam, first the incident beam is binarized together with phase tilt, then it is separated by a lens (which is part of a 4f system) into several diffraction orders where the $+1$ diffraction order is the exact Fourier transform of the desired field; this diffraction order is selected by a spatial filter and is subsequently retransformed by a second lens giving as result an inverted and tilted version of the desired field, which can be recovered by the use of a mirror. For the vector beam generation, the strategy followed differs mainly in the fact that the incoming beam is split into two orthogonally polarized beams and propagated by slightly different directions; additionally, the form of the incident wave is not plane but has been selected in a manner that additional equal and opposite phase tilts are introduced to its polarized components; the introduced tilts are chosen so that each component may be isolated from the diffracted orders by a spatial filter and overlapped on the Fourier plane. Radially and azimuthally polarized beams were generated with this method; one of the main disadvantages is the inefficient use of light.

To overcome the inefficient use of light detected in the work of Neil et all [88]; Maurer and collaborators proposed in 2007 an interferometric method, which allows amplitude and phase control at video rate switching, and is implemented with a nematic liquid crystal SLM to diffract a Gaussian laser beam [89]. In this approach the SLM

is divided into two halves, each displays a hologram, therefore the independent and simultaneous manipulation of each diffracted beam is possible by modifying the displayed hologram on the corresponding half. They use linearly polarized light at 45°, then the beam is separated in two outgoing beams with orthogonal polarization states separated by 2.5°, eventually the beams are expanded and diffracted at each half of the SLM for individual manipulation by the hologram that are controlled by a computer in real time, finally both beams are recombined to create the vector mode. The optical path traveled by both beams between splitting and recombination is almost the same, providing the system with high stability. The holograms are calculated from the analytical form of the desired beams and are designed to fulfill two conditions: transforming the incoming beams into the selected modes; and reverse exactly the propagation direction of the incoming beams into their respective first diffraction orders. With this configuration Hermite–Gaussian and Laguerre–Gaussian vector beam modes of different order are generated, potential applications include material processing, STED microscopy and optical tweezers. The main drawback of this approximation is that it works well only for a restricted group of modes, whereas for pronounced amplitude profile modes, the contrast of the holographic grating structure should be modulated with its amplitude profile.

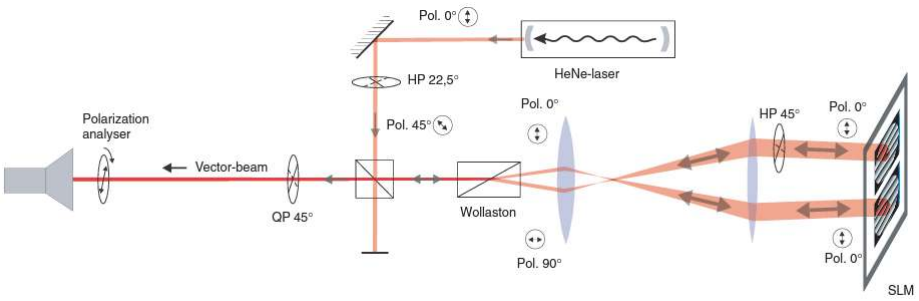

FIGURE 3.5: Experimental setup used by Maurer and collaborators, taken form [89]. Notice that the input beam is split in two orthogonally polarized beams by a Wollaston prism, then each component hits a different part of the SLM in order to be modulated before recombination.

In their work, Arrizón and collaborators (2007) [90] presented 3 classes of phase CGH (one of them already reported in the literature and two of them new proposals) to encode scalar complex fields, two of them give high quality beams even when implemented in low-resolution SLMs: Laguerre-Gauss and non-diffracting Bessel beams are successfully produced. The implementation is performed using a translucent twisted-nematic liquid-crystal SLM (the LC2002 SLM of HoloEye Photonics AG) in a phase-mostly configuration with a phase range reduced to $1.2\pi rad$, two linear polarizers, a quarter-wave plate and a CCD camera to record the intensities distributions of the generated beams. The proposed technique may have applications in manipulation of living cells with optical tweezers.

Another approach, also published in 2007 [91], involves the use of a transmissive twist nematic liquid crystal SLM implemented in a $4-f$ system with an interferometric array to generate arbitrary vector beams. For this case, the hologram with the appropriate phase distribution (depending on the desired beam) is designed and displayed on the SLM in such a way that the incoming beam may be diffracted into several diffraction orders, spatially filtering only the $\pm$ first orders to be converted into the circular polarization base (each one to each orthogonal component) and then

recombined by a Ronchi phase grating; special care is taken to make the period of the hologram match as much as possible with that of the Ronchi grating. The technique showed in this work permits the codification for different beams in different areas of the SLM allowing for a single vector beam to contain multiple polarization configurations.

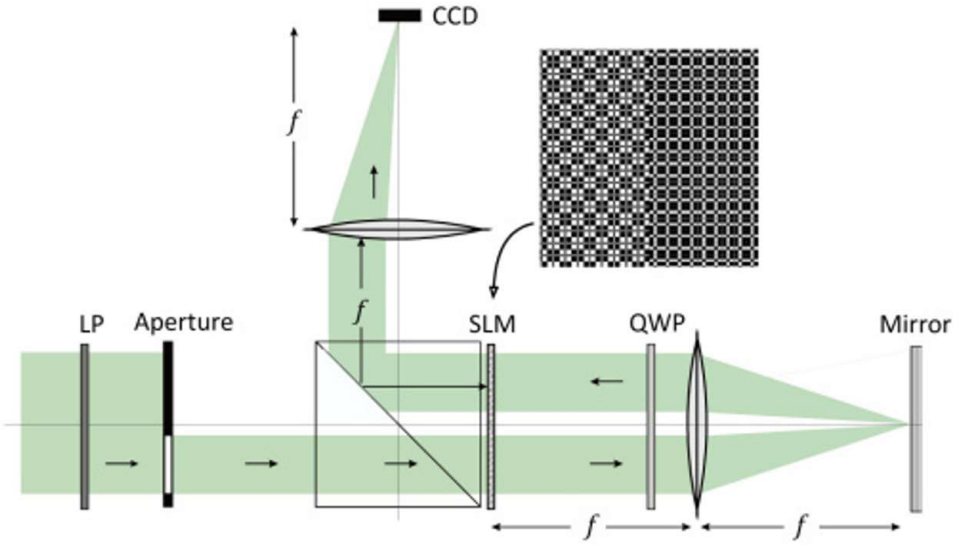

FIGURE 3.6: Experimental configuration for the double pass configuration, taken from [92]. By the first pass one polarization component is fully modulated by the proper codification of a binary phase grating; then the beam passes twice a QWP to rotate the polarization states by 90° upon reflection, finally the second pass on the SLM permits the modulation of the other polarization component.

The work of Moreno and collaborators (2011) shows the possibility of having full spatial polarization modulation [92]. In their set up the main element is a parallel aligned nematic SLM manufactured by Seiko Epson, operated in a transmissive mode and light with polarization states in both components: horizontal and vertical. They report in detail the different stages of the experiment: first they studied the possibilities of phase and amplitude control after a single pass (by using a linear phase grating with encoded amplitude); then they focus on the double modulation approximation (which requires swapping the orthogonal polarization components) using a single SLM divided in two working areas and operated in a reflective configuration, the experimental configuration is shown on figure 3.6. Their approach requires two major features: first to encode the optical elements onto the SLM; second to rotate the polarization states by 90° which allows full control over the zeroth and first diffraction orders, it is important to emphasize that only one polarization state is affected on each pass and the orientation and period of the grating that gives the second modulation can be the same or different from the first one. The authors suggest options for equivalent configurations using two SLMs either in the reflective or transmissive mode. The correct alignment of the system is essential to avoid interference fringes. Finally, the resolution is limited by the number of pixels on the SLM and their size.

In 2014, Zhu and Wang [69] proposed a technique (the experimental setup is shown on figure 3.7) that allows the arbitrary manipulation of phase and amplitude of an

incident beam by the use of two Holoeye PLUTO phase-only SLMs based on reflective LCoS micro-displays; to achieve their goal, they required to control the polarization direction of the input light on the first and second SLMs. Considering that each SLM imprints an specific phase distribution $\phi_1(x,y)$ (which determines the amplitude distribution) and $\phi_2(x,y)$ respectively (a linear combination of $\phi_1(x,y)$ and $\phi_2(x,y)$ determines the final phase distribution), it is possible to calculate the theoretical electrical field of the desired beam to determine the corresponding phase patterns to be loaded on each SLM. With this approach the generation of LG beams, Bessel beams, collinear OAM beams and arbitrary beams with odd-shaped intensity was successfully shown. The authors suggest applications in free-space optical communications.

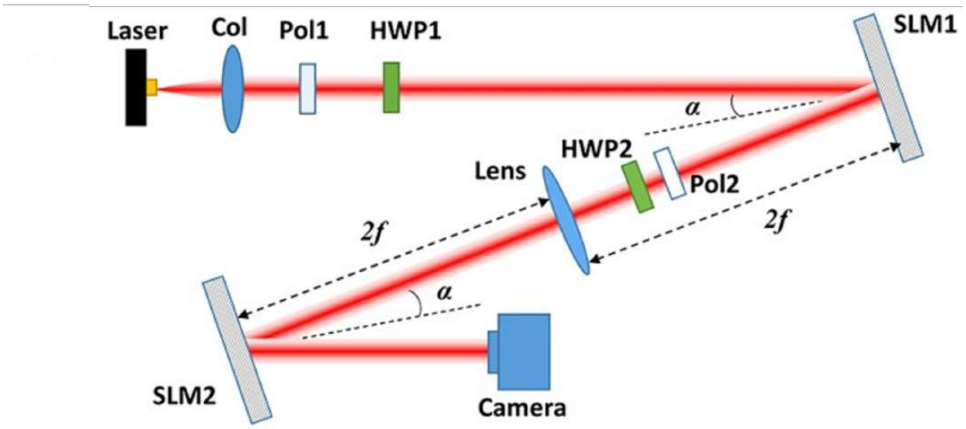

FIGURE 3.7: Experimental setup using two SLMs to achieve arbitrary phase and amplitude manipulation. The hologram on SLM1 gives the amplitude distribution while a combination of holograms in SLM 1 and SLM2 provides the phase distribution. Col: collimator, Pol: polarizer, HWP: half-wave plate. Taken from [69].

A work of 2015 by Chen and collaborators [93], demonstrates the simultaneous control of amplitude, phase and state of polarization by implementing a transmissive phase-only SLM in a 4f system, using a macro-pixel encoding approach (each macro-pixel composed by four pixels). The digital holograms that creates the two orthogonally polarized beams are created by codifying the complex amplitude distribution using complex amplitude decomposition (that is, considering it as a sum of two complex quantities with constant module) in a phase-only pattern that have the ability to encode arbitrary phase and amplitude distributions. Here, two orthogonally polarized components are passed through the SLM, which provides them structured amplitude profile and phase distributions, afterwards they are coaxially superimposed to create the vector beams. The authors present this implementation as promising in applications such as focus shaping, high-resolution imaging and optical tweezers.

Taking advantage of the superposition principle in optics, Rosales-Guzmán, Bhebhe, and Forbes accomplish in 2017 [94] the generation of several (up to sixteen) vector beams with varied polarization distributions and spatial shapes simultaneously by using a multiplexing approach and implemented with a single reflective SLM (Holoeye PLUTO). Their approach is an interferometric approximation that relies on dividing the wavefront of the initial beam, which comes from a horizontally polarized laser. On the SLM two sets of scalar fields are created, each with a unique carrier frequency, which is selected in such a way that two groups of beams may be formed:

each group will follow different paths to acquire orthogonal circular polarization; with the proper codification of the hologram it is possible to digitally and simultaneously manipulate the phase, amplitude and shape of each beam previous to recombination by pairs. Finally the beams are recombined into a single set by coaxial superposition, using a polarizing beam splitter. To verify their technique, they generate Bessel modes and cylindrical vector beams. The applications envisaged by the authors include optical communications and quantum computing.

In 2018 Otte and collaborators [95] presented a new technique based on spatial multiplexing of several holograms with two quarter-wave plates and a reflective phase-only SLM passing the beam twice to maintain the full resolution of the SLM (because it is used in full-screen mode), that allows manipulation of phase, polarization, and amplitude: after the first pass, the encoding of amplitude and phase is performed (here the first diffraction order is used); while the second pass (using the zeroth diffraction order), structures the polarization properties. This is not an interferometric method, but a single-beam one that requires the generation of advanced (sophisticated) holograms to enable the manipulation of the DoFs of light and produce the tailored beams. The spatial resolution is given by the period of the blazed gratings encoded into the holograms and not by SLM properties. Applications are focused on optical trapping, laser material machining and advanced imaging techniques.

Forbes, Dudley, and McLaren [75] give a complete review of approaches, known up to 2016, to create structured light by complex amplitude modulation on phase-only SLMs (this approach will be explained in more detail in the next chapter). Among the applications, they spotlight those in the fields of creating non-diffracting Bessel beams, vortex beams carrying OAM, vector beams, optical trapping and tweezing, multiplexing approaches in free space and fibers; they also point out the relevance of this techniques in classical and quantum information.

Chapter 4

Complex Amplitude Modulation.

On this chapter a brief overview concerning complex amplitude modulation (CAM) methods to shape light for different purposes is presented, pointing out the diversity of approaches. The main concepts needed to understand this method are also shown, particularly the proposal of 2007 by Arrizón et al [90] (used in this work) is developed in more detail.

Complex Amplitude Modulation (CAM) is a sophisticated technique widely used in diverse fields of optics, photonics and signal processing, due to its capability to control with high precision the phase and amplitude of a given light field, enabling the generation of customized and tailored optical beams that include scalar beams, vector beams and arbitrary amplitude distribution beams. The key of CAM relies on how the phase and amplitude information is encoded.

CAM is not a new or recent approach, the concept was slowly developed by contributions of several scientists and was favored with technological advancements; some of the fundamental concepts in this regard go back to the conceptualization of light as a wave and include wavefront engineering and holography. The latter was a concept introduced by Dennis Gabor in his seminal work "A new microscope principle" in which he showed that optical information may be transposed into variations of optical path difference, or, alternatively, into amplitude and phase distributions [96]. The advent of computer generated holograms (CGH) revolutionized the implementations of this technique enabling real-time manipulation of light, which combined with the deeper understanding that researchers achieve about light's behaviour have positioned CAM as a priceless technique concerning light shaping for different applications such as communications [14], microscopy [13], and laser processing [97].

Before explaining the fundamental concepts related with CAM, it is necessary to answer the following questions: what happen with light when it passes through an optical element and what the effect of a grating is? These two phenomena will be crucial to understand CAM. First, In general when light interacts with matter,in the specific case of light passing through an optical element, one or more of its properties may be modified according to the characteristics of the element but in general part of the light may be absorbed (leading to changes in the intensity), part of the light will be transmitted, and also it will experience a phase change due to the interactions with the material (see figure 4.1); the properties and behavior of some optical elements (such as mirrors, lenses, or diffractive elements) is well known and, in some cases, the effects that such element will have in a wavefront, may be simulated and codified into a CGH. Second, a grating may be described as an optical element with a periodic structure consisting on transparent and opaque slits; when interacting with

a grating, light experiences diffraction, which leads to the separation and redirection of the incident light into multiple diffraction orders; "in a sense, nature converts the phase changes into intensity changes through diffraction (...) thus by exploiting this principle further it is possible to structure arbitrary amplitude, phase and polarization" [5]. CAM involves the manipulation of the phase across a spatial domain, to achieve so the phase distribution should be modeled into a CGH to control the direction and intensity of the diffraction orders by codifying an appropriate phase profile.

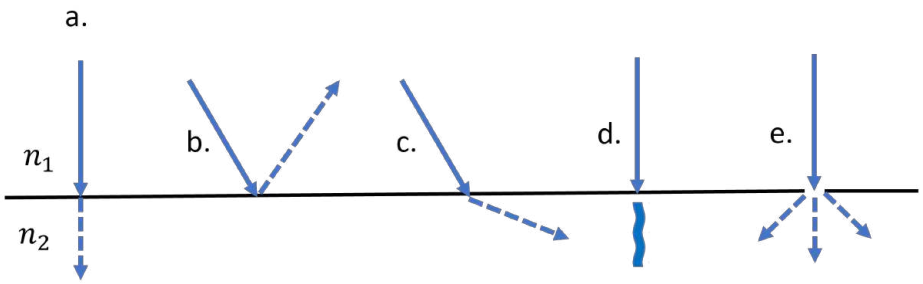

FIGURE 4.1: Phenomena that light may experience when interacting with optical elements: a) transmission, b) reflection, c) refraction, d) absorption, and e) diffraction. In the figure n_1 is the refraction index of the medium and n_2 is the refractive index of the optical element.

4.1 Complex Amplitude Modulation approaches

As stated on the previous chapter, most of the SLMs commercially available modulate only or mostly either the phase or the amplitude of light, nevertheless for many applications specific control over both DoFs of an input field is required to obtain the desired field. In this context, complex amplitude modulation (CAM), which can be understood as the possibility "to control the amplitude and the phase of the incident illumination independently (...) which assumes the need of at least two physical modulation processes" [17], emerges as a powerful and versatile tool.

Phase-only modulation is used when the amplitude distribution of the desired field is expected to be the same as that of the input field and "implies that the state of polarization of modulated waves remains intact" [98], examples of phase-only modulation include redirection or inclination of the beam, focusing, and providing the beam with orbital angular momentum; to achieve this type of modulation the hologram is codified as $mod[\phi_2 - \phi_1, 2\pi]$, where ϕ_1 is the phase of the input field and ϕ_2 is the desired phase; a disadvantage of phase-only modulation is that it produces undesired secondary rings. On the other hand, amplitude-only modulation is the case when only a change in the amplitude distribution of the beam is desired; usually, if a phase-only SLM is going to be used to modulate the amplitude, it can only be decreased by distributing the light away from the desired order in a spatially-dependent way, therefore controlling the depth for each point allows amplitude modulation. Controlling amplitude and phase simultaneously may be achieved by CAM.

The phase-only, amplitude-only or complex-amplitude response of a device can be represented in a complex plane. Recall that a complex number is expressed in its standard form as $a + bi$, where a is the real part and b is the imaginary part; and

in the exponential form a complex number is given by $r\exp^{i\theta}$, where r is the magnitude and θ is the phase; both representations are related by $r = \sqrt{a^2 + b^2}$ and $\theta = arctan(\frac{b}{a})$. That being the case, the phase-only response corresponds to change θ while keeping r constant, this can be represented as a rotation around the origin while maintaining constant the distance to the origin, or a unit circle traced in the complex plane; on the contrary, an amplitude-only modulation corresponds to changing r while keeping θ constant, which can be understood as moving across a straight line that makes an angle θ with respect to the x-axis; finally, complex amplitude modulation modifies the values of both r and θ can be viewed as changing positions inside a filled circle in the complex plane (see figure 4.2).

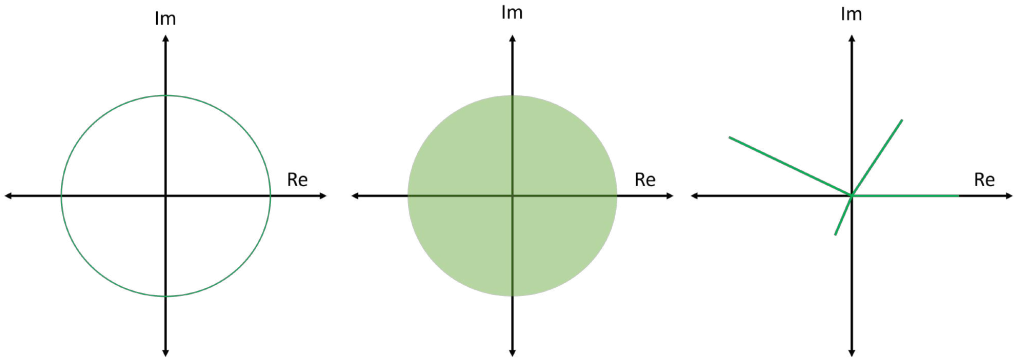

FIGURE 4.2: Representation in the complex plane of a phase only response, which traces a unit circle in the complex plane (left); an amplitude-only response, in the drawing each line represent a different wavefront with specific phase and amplitude (right); and a complex-amplitude modulation response, which corresponds to a filled circle (middle).

The general scheme of complex amplitude modulation consists on representing the amplitude and phase of a given field as a complex number (a specific position in the complex plane); then it is necessary to determine the desired complex amplitude distribution and encode it, that is assign the specific values for phase and amplitude at each point; afterwards, the modulation pattern that specifies how the amplitude and phase must change across the wavefront must be generated, which allows the creation of the desired field; use a device (generally a SLM) to display the modulation pattern; finally light should be directed to the SLM and after interacting with it, the field with the desired phase and amplitude distribution is created.

For example, consider that given an optical field of the form

$$E_{in}(x,y) = A_{in}(x,y)e^{i\phi_{in}}, \tag{4.1}$$

which is supposed to be transformed into a desired field

$$E_{des}(x,y) = A_{des}(x,y)e^{i\phi_{des}}, \tag{4.2}$$

in a single step. This requires an element with a transmission function that has phase as well as amplitude modulation and which is given by

$$t = \frac{A_{des}}{A_{in}}e^{i(\phi_{des}-\phi_{in})} = A_{rel}e^{i\phi_{rel}}, \tag{4.3}$$

but expressed as a form that is phase-only dependent such as

$$t \rightarrow \exp[i\Phi_{slm}(A_{rel}, \phi_{rel})]. \tag{4.4}$$

One implication of the latter equation is that the desired beam is created at the plane of the SLM but, for practical reasons, an optical system (usually a telescope) is generally used to rely the SLM's plane to a detector plane. Notice two important things concerning the transmission function: first, that the expression for Φ_{slm} considers variations of amplitude in a position-dependent manner; second, it results evident that encoding is critical since "accurate control of the optical field crucially depends on the method employed to encode the hologram" [99].

In general, techniques that use this approach, require spatial filtering to select the desired diffraction order either if light was sent to the zero order (by decreasing the depth of the phase step) or to higher diffraction orders (by adding a high-frequency grating) [5, 75, 100]. In traditional approaches, the transformation of the field is achieved by diffractive optical elements executed in two steps with phase-only optics, first modifying the amplitude and then correcting the phase [75]

Once clearly stated that the transmission function encoded in the hologram must contain phase and amplitude modulation and that this can be achieved by CAM approach, it turns out necessary to mention that it is precisely the different ways of finding $\Phi_{slm}(A_{rel}, \phi_{rel})$ and the manner of implementing it what gives the numerous approaches to CAM. For example, "the phase-only complex amplitude modulation scheme for low resolution devices, such as SLM, originates from the report of Kirk and Jones (in 1971)" [101]. In their work, Kirk and Jones, present for the first time a phase-only filter with arbitrary signal-to-noise ratio, minimization of plotting, and ease of replication. Their complex-valued spatial filter is fabricated holographically by encoding phase (as a phase retardation) and amplitude (by varying the depth of modulation of a superimposed phase grating) together and allows the modulation of both amplitude and phase of a wave front incident on it [17]. Remarkably, the behavior of this filter can be made as close to that of an ideal filter as desired.

The different approaches to CAM can be broadly divided into two categories [102]: those focused on the number of devices used (single or multiple SLMs) and those centered on the encoding method (super-pixel approach, double constrain iterative method, hologram bleaching, and double-phase hologram). It is important to consider that independently of the variation used to implement CAM, it "is realized with the reduction of effective resolution because the amount of information of a complex hologram doubles that of an amplitude-only or phase-only hologram. In other words, the essence of CAM is sacrificing spatial bandwidth product to achieve the expression of complex amplitude information" [102]. From the work of Bartelt [103], which proposes a suitable configuration of two pure-phase filters and additional optical elements that allows amplitude and phase control with 100% efficiency, further approaches using multiple SLMs were among the first proposals to achieve CAM, nevertheless they resulted in bulky setups that require a precise alignment, which can be hard to achieve.

Within the classification of multiple SLMs to achieve CAM are the cascaded methods, the interferometric methods; and the iteration and phase compensation method. The former consists on the use of two liquid-crystal devices to consecutively modulate amplitude and phase, such as the work of Gregory and collaborators in which two liquid-crystal screens are used [104], the proposal of Amako and collaborators

[105], and the slightly more recent approach given by Hsieh and collaborators, that uses a commercially available cascaded twisted nematic liquid crystal SLM [106]. Interferometric methods such as [107] and [108] rely on the interferometric superposition of light, in this approaches the hologram is decomposed in two amplitude-only holograms (AOHs) or phase-only holograms (PHOs) each one uploaded in a different SLM, and can include Mach-Zender interferometer, Michelson interferometer, common-path interferometric schemes or others. The iteration and phase compensation method which also uses two SLMs: the first to obtain the target amplitude (by an iterative algorithm), and the second to compensate the phase reconstructed by the first one [109]. On the other hand, single SLM approximations are more recent, and avoid the complicated setups of the multiple SLMs approaches, in this classification works as [92] or [94], are included and consider either dividing the SLM's screen into two halves or multiplexing approach.

Concerning encoding methods: for super-pixel (also known as macro-pixel) approach several pixels of the device constitute a pixel for the desired complex amplitude distribution, in [110] for example, a double-phase hologram is implemented in an available low-resolution SLM to achieve complex amplitude modulation with macro-pixels composed by arrays of 1x2 and 2x2 pixels; the double constrain iterative method is based on iteration through suitable algorithms to restrict phase and amplitude over each iteration, usually employing PHOs, in [111] the phase-only computer generated hologram is calculated by a double-constrain Gerchberg–Saxton algorithm to constrain amplitude and phase in the image plane, further correction in the image plane is performed, a drawback of this approaches is that iterations result time-consuming; for hologram bleaching the information of the amplitude is encoded as part of the phase information after the target complex amplitude interferes with an off-axis reference plane wave, in this approach the desired beam is found on the first diffraction order; lastly the double-pass approach is a method based on a single-pixel approximation where the complex field is decomposed in two POHs and complementary checkerboard patterns to combine them into a phase-only SLM, as in [112] where a 4f system is used for the complex field reconstruction after applying a low-pass filter at the Fourier plane, an advantage is the high computational efficiency but on the drawbacks it has lower reconstruction accuracy than super-pixel methods since the reconstruction is affected by the information of adjacent pixels.

In their work "Comparison of beam generation techniques using a phase only spatial light modulator" [100], Clark and collaborators test both numerically and experimentally six hologram generation techniques for a single Laguerre-Gaussian beam, an optical Ferris wheel, and a photographic image known as "Laser class sailboat" (see figure 4.3). After analysis, they ranked the perform of the six methods according to the obtained mode quality and power; the six selected methods rely on the use of phase gratings (the desired field is found on the first-order deflection and must be spatially selected), are deterministic and based on single-pass. In their findings and conclusions the authors state that "Method F", which corresponds to the proposal of Arrizón and collaborators [90], gives the best results concerning the numerical analysis, produces accurate representation of the fields for all tested modes (and also for the picture), and besides performing well, it has the advantage of requiring reduced phase range, which allows the use of this technique with low-cost SLMs.

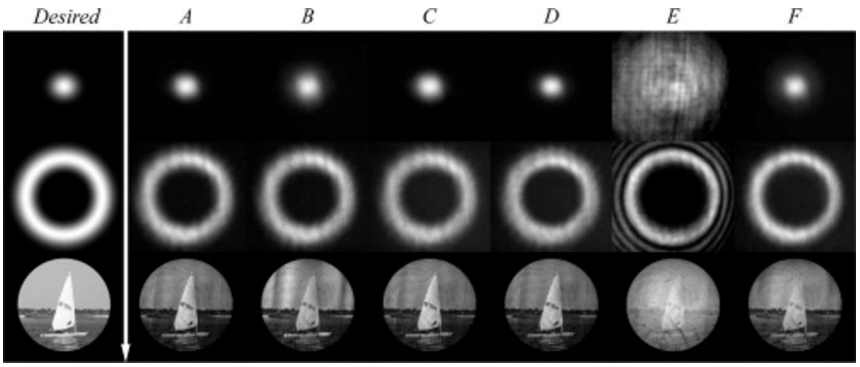

FIGURE 4.3: Measured intensities for a fundamental Gaussian, a LG_1^0 and the laser class sailboat. First column shows the desired pattern. First and second rows were measured after one Rayleigh range, the last row shows measurements performed in the image plane of the SLM.

4.2 The proposal of Arrizón.

As already emphasized, when referring beam shaping, amplitude and phase modulation is critical. CAM may be achieved by encoding amplitude information as phase information thus allowing the independent control of both DoFs. One of the approaches that does precisely this, and which has been found to give excellent results in field reconstruction, is the proposal of Arrizón and collaborators [90]. What follows is a scheme of their proposal with brief comments, and some added details. It is important to notice that this scheme is presented to generate scalar fields, but it can be generalized to the generation of vector beams since these are a superposition of the former as long as the two scalar beams are spatially orthogonal and with orthogonal polarization states.

Given an input beam, the goal is to obtain a desired beam specified by an amplitude term, $A(x,y) \in [0,1]$, and a phase term, $\phi(x,y) \in [-\pi,\pi]$, as:

$$s(x,y) = A(x,y)\exp[i\phi(x,y)]. \tag{4.5}$$

For this purpose, the desired beam must be first expressed by means of a phase CGH, which transmittance may be expressed as a function that explicitly depends on the amplitude and phase of the desired field:

$$h(x,y) = \exp[i\Psi(A(x,y),\phi(x,y))]. \tag{4.6}$$

It is clear that the key to obtain the desired hologram is establishing $\Psi(A,\phi)$, which can be achieved by several means. The strategy followed in the cited work is proposing a Fourier series representation of $h(x,y)$ in the domain of ϕ:

$$h(x,y) = \sum_{q=-\infty}^{\infty} h_q(x,y) = \sum_{q=-\infty}^{\infty} c_q^A \exp(iq\phi), \tag{4.7}$$

where, as conventionally, the coefficients

$$c_q^A = (2\pi)^{-1} \int_{-\pi}^{\pi} \exp[i\psi(A,\phi)] \exp(-iq\phi) d\phi. \tag{4.8}$$

By imposing the signal encoding condition ($c_1^A = Aa$ for some positive constant a), then the desired field distribution may be recovered from the term $h_1(x,y)$. Considering the expression for the coefficients c_q^A, the explicit form of the term c_1^A is given by:

$$c_1^A = (2\pi)^{-1} \int_{-\pi}^{\pi} \exp[i\psi(A,\phi)] \exp(-i\phi) d\phi = \int_{-\pi}^{\pi} \exp[i\left(\psi(A,\phi) - \phi\right)] d\phi = Aa, \tag{4.9}$$

which can be rewritten as:

$$c_1^A = \int_{-\pi}^{\pi} (\cos[(\psi(A,\phi) - \phi] + i \sin[(\psi(A,\phi) - \phi]) \, d\phi = 2\pi Aa. \tag{4.10}$$

In other words, the signal encoding condition is fulfilled if:

$$\int_{-\pi}^{\pi} \cos[(\psi(A,\phi) - \phi] d\phi = 2\pi Aa, \tag{4.11}$$

$$\int_{-\pi}^{\pi} \sin[(\psi(A,\phi) - \phi] d\phi = 0. \tag{4.12}$$

Since the maximum of equation 4.11 is 2π, the maximum value of a in the encoding condition is determined to be $a = 1$. On the other hand, the condition 4.12 is fulfilled if $\psi(A,\phi)$ has odd symmetry in ϕ. Notice that the solution is not unique. In the work that is being analyzed, three different sets of functions, which lead to three different types of phase computer generated holograms, are presented. Those solutions are listed below:

1. First type: A CGH equivalent to a synthetic hologram that can be found in literature previous to the work of Arrizón et al is given by $\Psi(A,\phi) = f(A)\phi$, therefore the expression for c_q^A may be rewritten as:

$$c_q^A = (2\pi)^{-1} \int_{-\pi}^{\pi} \cos[(f(A) - q)\phi] d\phi, \tag{4.13}$$

that is:

$$c_q^A = (2\pi)^{-1} \left(2 \frac{\sin[(f(A) - q)\pi]}{(f(A) - q)\pi} \right), \tag{4.14}$$

which corresponds to:

$$c_q^A = sinc[f(A) - q]. \tag{4.15}$$

Given the fact that the sinc function is an even function, the coefficients can be written:

$$c_q^A = sinc[q - f(A)]. \tag{4.16}$$

For the encoding condition $c_1^A = Aa = sinc[1 - f(A)]$, and for $a = 1$:

$$A = sinc[1 - f(A)]. \tag{4.17}$$

The function $f(A)$ is obtained by numerical inversion of 4.17.

2. Second type: Corresponds to a CGH presented in [90] for the first time. A function of the form $\Psi(A, \phi) = \phi + f(A) \sin\phi$, which is a valid proposal due to the odd symmetry in ϕ. Considering this, the phase CGH transmittance, according to 4.6 is given by $h(x, y) = \exp[i\phi + if(A) \sin\phi]$, which can be written alternatively as:

$$h(x, y) = \exp(i\phi) \exp[if(A) \sin\phi]. \tag{4.18}$$

Using the Jacobi-Anger identity, the second term in 4.18 may be written as:

$$\exp[if(A) \sin\phi] = \sum_{q=-\infty}^{\infty} J_q[f(A)] \exp(iq\phi), \tag{4.19}$$

where $J_q[f(A)]$ is the Bessel function of integer-order q. Considering this expression in 4.18 and the Fourier series expansion as expressed in 4.7:

$$\exp(i\phi) \sum_{q=-\infty}^{\infty} J_q[f(A)] \exp(iq\phi) = \sum_{q=-\infty}^{\infty} c_q^A \exp(iq\phi). \tag{4.20}$$

By considering the left side of 4.20, including the term $\exp(i\phi)$ in the summation and shifting the index of that summation (only on the left side) to $q \to q - 1$:

$$\sum_{q=-\infty}^{\infty} J_{q-1}[f(A)] \exp(iq\phi) = \sum_{q=-\infty}^{\infty} c_q^A \exp(iq\phi), \tag{4.21}$$

from which it can be seen that the coefficients $c_q^A = J_{q-1}[f(A)]$. For the encoding condition:

$$c_1^A = A = J_0[f(A)]. \tag{4.22}$$

Relation 4.22 is satisfied for $A \in [0, 1]$ and an appropriate value of $f(A) \in [0, x_0]$, where $x_0 \approx 2.4048$ is the first positive root of $J_0(x)$. As for the case of the holograms in the first type, $f(A)$ is found by numerical inversion of $c_1^A = A = J_0[f(A)]$.

3. Third type: Also corresponds to a CGH presented in [90] for the first time. A function with odd symmetry in ϕ and similar to the one used for obtaining the second type holograms is proposed: $\Psi(A, \phi) = f(A) \sin\phi$. Proceeding as in the previous case:

$$\exp[if(A)sin\phi] = \sum_{q=-\infty}^{\infty} c_q^A \exp(iq\phi). \tag{4.23}$$

By using again the Jacobi-Anger identity:

$$\sum_{q=-\infty}^{\infty} J_q[f(A)]\exp(iq\phi) = \sum_{q=-\infty}^{\infty} c_q^A \exp(iq\phi). \tag{4.24}$$

From which it can be seen that $c_q^A = J_a[f(A)]$. For the encoding condition:

$$c_1^A = Aa = J_1[f(A)]. \tag{4.25}$$

Equation 4.25 is fulfilled for a maximum value of $a = 0.5819$, which corresponds to the maximum value of $J_1(x)$ and occurs at $x = x_1 \approx 1.84$. Once again, $f(A)$ is obtained by numerical inversion. This approach may be implemented with phase modulation in a reduced domain, which implies that it can be easily obtained with conventional LC SLMs.

Chapter 5

Experimental implementation of CAM in an on-axis configuration.

In this section a description of the experimental setup implemented to generate Laguerre-Gauss vector beams in an on-axis configuration with the support of a SLM using CAM is provided. In the same manner, the algorithm to generate the holograms as well as the algorithms used for the characterization of the obtained modes are explained.

5.1 Experimental setup for the generation of LG vector beams.

The LG vector modes that have been described in previous chapters, were successfully generated by using an experimental setup in which two main elements were implemented: a SLM, which is used to project the holograms that will perform the CAM, the phase modulation and the beams' superposition; and a camera that is used for monitoring the beam and also as a mean to perform the intensity measurements required for the beam characterization. It is important to notice that single vector mode generation using a single SLM, as proposed for the first time up to our knowledge on this work, requires the beam to pass twice through the SLM to achieve independent manipulation of both polarization components, therefore the screen of the SLM was digitally divided in two halves.

Although it is true that, as mentioned on previous chapters, the use of SLMs to generate structured light is highly generalized, the main contribution of this work relies on the fact that the components that superimpose to generate the desired vector beam follow the same optical path (on-axis configuration), the manipulation is in both amplitude and phase by the use of complex amplitude modulation, and this is a single-beam generation approach, not a multiplexing one.

The SLM used for this implementation consists on a two-dimensional array of liquid-crysal pixels that for a known given reference (input) beam allows the specification of the desired (output) beam. Concretely it is a PLUTO 2.1 Holoeye device (which is shown in figure 5.1), which is a polarization-sensitive, reflective, phase-only LCOS which pixel pitch is $8.0\mu m$, active area of 15.36×8.64 mm, the fill factor is 93%, it achieves input frame rates of $60Hz$, finally although the total resolution of the SLM is 1920×1080, the screen was digitally divided in two, so the effective resolution for our implementation is 960×1080 pixels. Each pixel on the array acts as a programmable phase shifter depending on the assigned voltage (gray value). The SLM was controlled with Matlab via HDMI connection to the computer.

FIGURE 5.1: Picture of PLUTO 2.1 Holoeye SLM device.

The camera is a Thorlabs CMOS DCC3240C (see figure 5.2) with a resolution of 1280×1024 pixels, pixel size of $5.3\mu m$ with an imaging area of 6.78×5.43 mm. The camera allows control of acquisition rate from 0.5 fps to 5.06 fps, and exposure time may be modified from 0 ms to 343.4 ms. To operate the camera, it must be connected via standard 5V USB 3.0 port to the computer and the ThorCam^{TM} software for Windows has to be previously installed. The camera and the SLM are controlled with the same computer simultaneously.

FIGURE 5.2: Picture of the camera Thorlabs CMOS DCC3240C used.

Next a detailed description of the setup as well as a guideline of how the generation technique works is provided. For clarification purposes, figures 5.3 and 5.4 show a schematic representation of the experimental array in two different views.

We will emphasize here that the vector beam generation using a SLM requires a proper codification of the desired beam to generate the correct holograms. The first half of the SLM has a hologram that allows CAM and generates the scalar beams that will be superimposed with the appropriate topological charge; the second half of the SLM corrects only the phase of one of the components, which allows the superposition to take place.

The first stage of the experimental mounting is used for the generation of the input beam and it consists on a horizontally polarized He-Ne laser ($\lambda = 633$ nm, $12mW$

of power) followed by a microscope objective $10X$, which expands the beam, right away the objective microscope, a lens L_1 ($f_1 = 100$ mm) is used to collimate the beam and obtain an approximately plane wave front. To select a portion of that wave front, a spacial filter is used.

The second stage is composed by lenses L_2 ($f_2 = 175$ mm) and L_3 ($f_3 = 400$ mm), which form a telescope that is used to create an image of the input beam just in the plane of the SLM. Given the fact that the SLM is polarization-sensitive, it is assured that the incident beam has horizontal linear polarization to be fully and correctly modulated by the hologram on the first half of the device. When the beam reaches the first half of the SLM two important things happen: 1) CAM takes place providing the beam with specific topological charge l_1, according to the codified hologram; and 2) the beam is diffracted into several diffraction orders (not shown in figure).

Among the diffraction orders, the first one contains the desired information, therefore it must be selected and separated from the undesired light; to achieve this a second spatial filter is used. Additionally, two plane mirrors M_1 and M_2 are placed to redirect the selected order to the second half of the SLM; since the beam reflects in two mirrors, there is no net change on its topological charge. Before reaching the second half of the SLM, a half-wave plate (HWP) with its fast axis oriented at 22.5° is used to rotate the polarization state of the beam from linear to diagonal (45°), the orientation of the HWP ensures equal magnitude of both polarization components. consecutively, a second telescope using L_4 ($f_4 = 300$ mm) y L_5 ($f_5 = 300$ mm) is implemented.

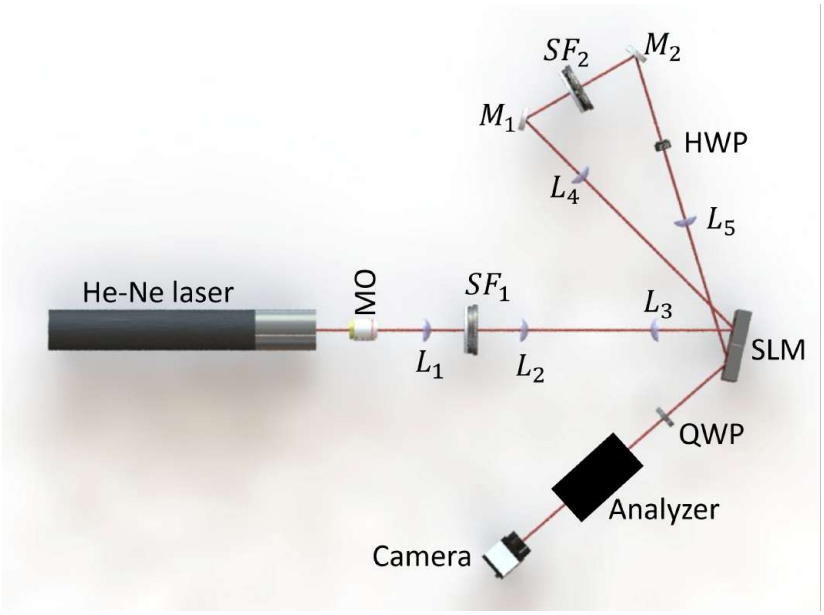

FIGURE 5.3: Schematic representation of the experimental setup. MO: microscope objective. L_i: Lenses. M_i: Mirrors. SF_i Spatial filters. SLM: Spatial light modulator. HWP: Half-wave plate. QWP: Quarter-wave plate.

Now the rotated beam reaches the second half of the SLM where a phase-only hologram is displayed and provides the beam with a different topological charge. Notice

that due to the polarization-sensitive nature of the SLM, only the horizontally polarized component of the beam will be modulated, while the vertically polarized component will remain unaffected. Recall that to achieve superposition, the two components must be orthogonal in both: amplitude distribution and polarization state. Therefore, for our case the horizontal and vertical component of the beam serve as a pair of base vector beams for the superposition process, which are collinearly recombined after the second reflection on the SLM.

After the SLM a quarter-wave plate (QWP), rotated at 45° with respect to the fast axis, is placed to perform a change on the polarization basis from the linear to the circular basis: horizontal polarization is converted into circular right-handed polarization, and vertical polarization into circular left-handed polarization.

Up to this point the vector beam has already been generated, nevertheless, two more elements are needed to monitor (camera) and characterize (analyzer) it. The analyzer is placed between the QWP and the camera, the description of how it is used will be provided in the following sections. Finally, the camera, which is connected to a computer, is used to verify alignment details and the intensity distribution of the generated beams.

Before starting with the measurements that will allow the characterization, it is necessary to verify that the beams are, in fact, vector beams. To do so, before placing the analyzer, a linear polarizer is situated between the QWP and the camera, then the polarizer is rotated and the change in the intensity distribution is the key to know if the beam is vector or scalar (as explained on Chapter 2).

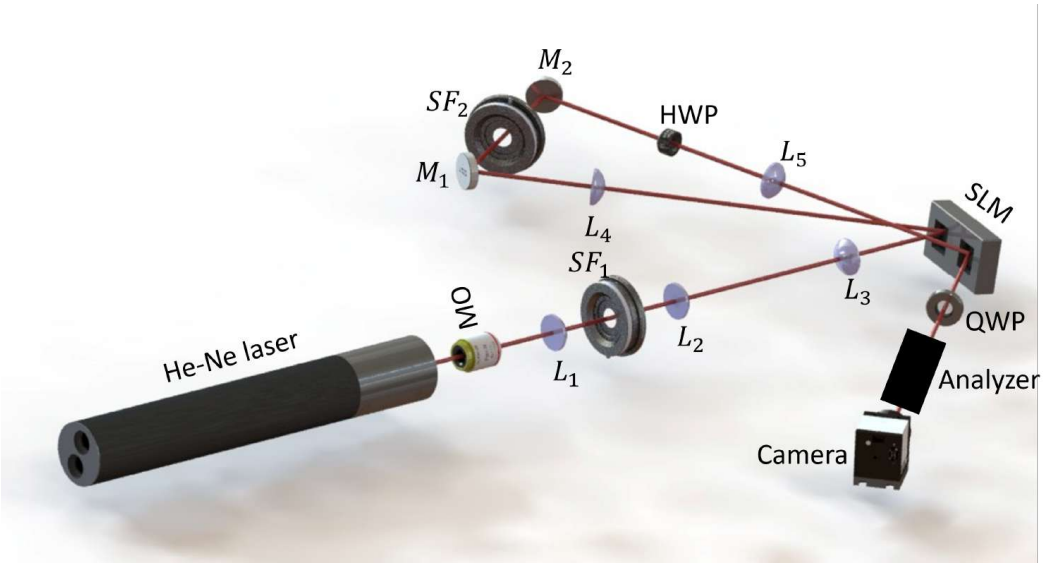

FIGURE 5.4: Schematic representation of the experimental setup. MO: microscope objective. L_i: Lenses. M_i: Mirrors. SF_i Spatial filters. SLM: Spatial light modulator. HWP: Half-wave plate. QWP: Quarter-wave plate.

With the technique described it is possible, in principle, to generate arbitrary vector fields by suitable codification of the holograms displayed on the SLM, nevertheless technical constrains still must be overcame and the scope of this work include only the generation of beams belonging to the family of the LG vector beams. In the next sections the details about hologram generation and beam characterization are described.

5.2 Hologram codification

As sated previously, the holograms were encoded using a Matlab algorithm. In our implementation the SLM screen is first divided in two halves, on the first half a CGH is codified using CAM as proposed in the "third type" hologram explained in [90]; the second half the CGH contains a blazed grating to perform phase-only modulation codified, as conventionally, through the modulo operation. The general scheme for the hologram codification is as follows:

1. First it is necessary to establish the resolution of the holograms, which must be the same as the resolution of the SLM, considering that two holograms will be displayed at the same time; thus digital division of SLM's screen is needed.
2. Two matrices, one for each half of the SLM, with the appropriate resolution are generated, in the same way all sizes are re-scaled to millimeters.
3. The beam parameters as well as the parameters needed to compute the LG scalar beam are defined. This parameters include: wavelength, wave number, beam radius, intermodal phase, topological charge and number of rings.
4. Amplitude and phase of the desired LG beam is computed. The hologram with the LG beam information is generated using CAM. To accomplish this, two functions are used: one to compute the Laguerre polynomials, the other to numerically invert $J_1[f(A)] = A$ and find $f(A)$.
5. The hologram with an azimuthally varying phase is generated.
6. After normalization of the gray levels to fully cover the available levels on the SLM, the two holograms are combined in a single image and displayed on the SLM.

In figure 5.5 three examples of the generated holograms are shown, it is important to emphasize that the sizes do not correspond to the sizes of the display in the SLM since it has been modified for clarity purposes.

5.3 Characterization of the generated beams

As stated on Chapter 2 Stokes polarimetry is a powerful technique that through Stokes parameters, which may be computed by four intensity measurements, represent a useful tool to determine not only the state of polarization of a beam but also to compute the concurrence, a quantity that determines the purity of a vector beam, and the orientation angle and flattening, parameters that will enable the stability analysis.

One at a time, each intensity measurement is taken with the camera and the obtained image is saved in .tif format for further processing. To perform the intensity measurements, the analyzer (which is composed by a linear polarzer and a QWP or a HWP) must be setted up at an adequate configuration, that is:

1. To measure I_R the beam passes through a QWP with its fast axis oriented at $+45^\circ$ followed by a linear polarizer with its transmission axis in a horizontal position, to finally reach the camera.
2. For the measurement of I_L the same configuration as in the previous case is needed, but in this case the QWP is rotated at -45°.

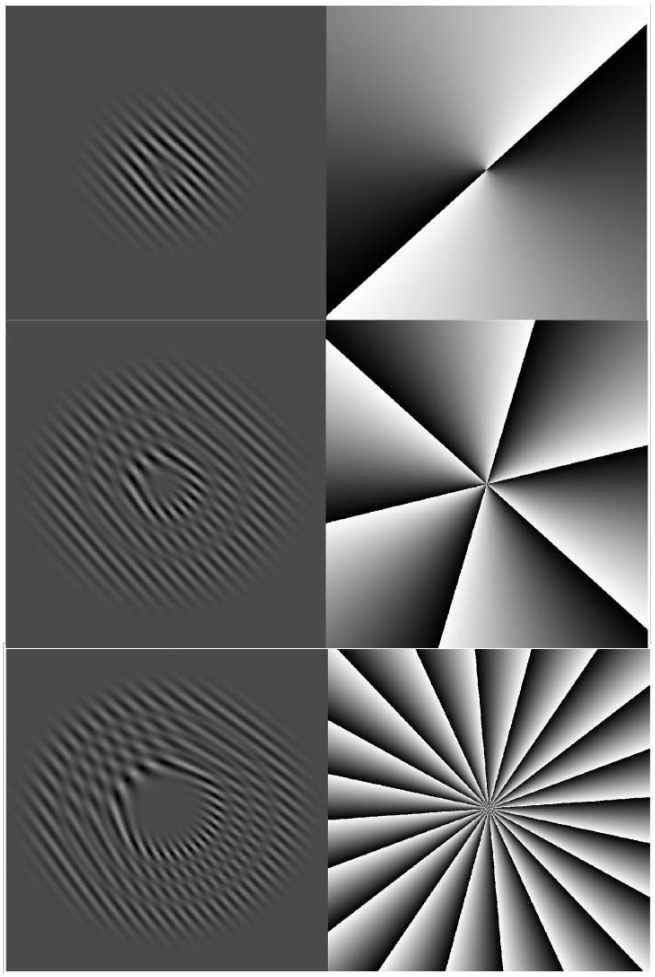

FIGURE 5.5: Holograms used to generate LG vector beams with different number of rings and topological charge. On the left CAM CGH, on the right POH. The values for the number of rings correspond (from top to bottom) to $p = 0, 2, 3$ and the values for the topological charge (from top to bottom) are $l = 2, 6, 20$.The display corresponds to the digital partition of the SLM available space.

3. For I_H the QWP is replaced by a HWP with its fast axis at 0°.
4. Finally, to measure I_D, the HWP is rotated at 22.5°.

Once all the measurements are recorded, those measurements are used to compute with Matlab the Stokes parameters as established by 2.32, further reconstruction of the transverse polarization distribution of the beams is possible by assigning, for each point on the image, a value of the angle of rotation and ellipticity (see equation 2.31). The purity of the generated beams is given by the concurrence as given in equation 2.35. Finally, to determine the stability of the beams, a comparison of the flattening and the orientation (as expressed in 2.37) is performed through the root mean squared error (RMSE), as usually defined, but considering the expected value as the value recorded for each beam on $t = t_0$; in the case of a beam that keeps the same flattening and orientation of its polarization over time, the corresponding values would be the same for t_0, t_1, and t_2. Ideally, the RMSE would be 0% for a beam that suffered no changes and 100% for a beam that changes completely, therefore, the closest the RMSE to 0%, the more stability the beam has. In all cases, the values were

compared with the expected values according to numerical simulations.

Chapter 6

Generation and characterization of Laguerre-Gauss vector modes

During the experimental implementation several combinations for different LG vector modes were generated. That is, we superimposed LG modes for values of $p = 0, 1, ..., 4$ and $l = \pm 1, \pm 2, ..., \pm 4$ in all the possible combinations, obtaining as can be seen on the figures displayed along this chapter that:

1. As the number of rings is increased, the spot size is increased too. For values with $p > 2$ the spot size was too big that it was not possible to be captured entirely by the camera, because part of the spot was too near to the edges. This complication may be overcame by reducing the spot size, using a camera with larger sensor or capture multiple shots and merge to reconstruct the whole transversal section of the beam. In spite of this inconvenience, for the purposes of this thesis it is not necessary to generate beams with high values of p, since the main goal is to demonstrate that the proposed technique works and this is achieved by generating vector beams regardless of the values of the parameters for the topological charge and the number of rings.

2. As the topological charge is increased, more discontinuities appeared when I_R and I_L where measured and instead of showing a continues ring (or concentric rings) as expected, a doted circumference (or concentric doted circumferences) was encountered. This may be caused by analyzer misalignment, calibration issues in the wave plates implemented in the experimental set up, or beam distortions due to optical path followed by the beam; which can be overcome by the use of optical devices with more quality and ensuring the correct calibration of the instruments used. As with the number of rings, high values of topological charge are not mandatory since the goal of the reported work is a proof-of-principle of the technique.

To evidence the effectiveness of the technique, in this work we report five representative beams illustrating the cases of modes with different intermodal phase and modes with topological charge higher than 1 and number of additional rings higher than zero (see figures 6.1 and 6.2). For the characterization, four different measurements of intensity were performed, each associated with a polarisation state: horizontal (I_H), diagonal (I_{+45}), right-handed (I_R) and left-handed (I_L). The images acquired with those measurements were processed in a dedicated Matlab code that we wrote, as detailed on Chapter 5, to determine Stokes parameters, which were used to reconstruct the transverse polarisation distribution as well as to calculate the vectorness, polarisation angle, and flattering of each beam.

6.1 Generation

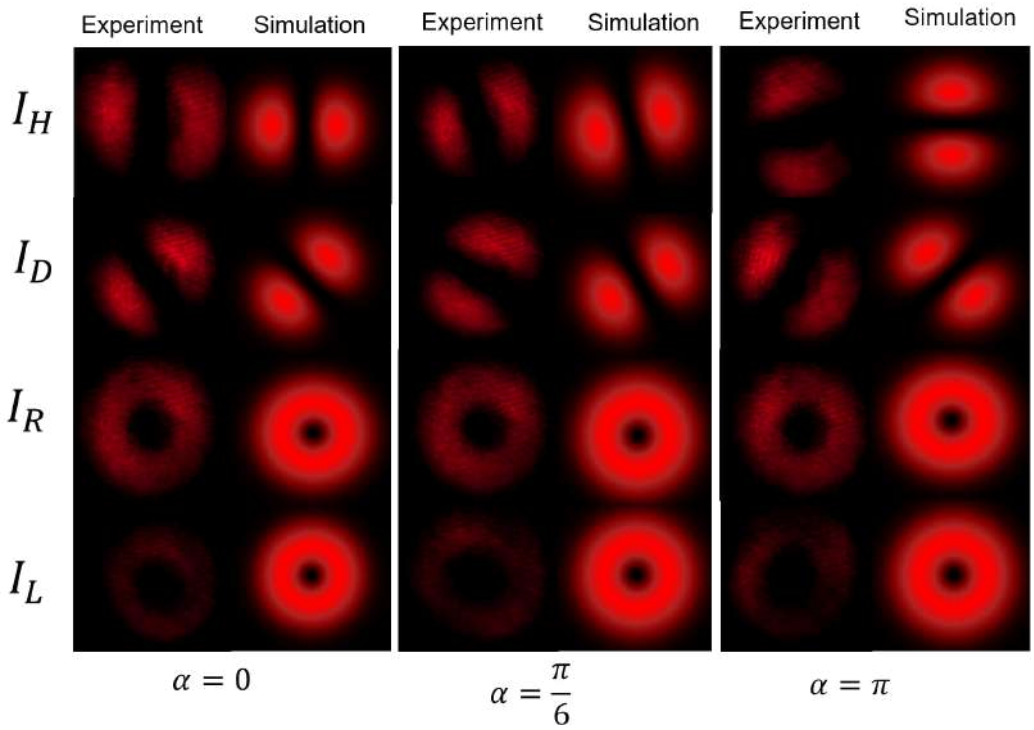

FIGURE 6.1: Vector mode $\frac{\sqrt{2}}{2}\left(LG_0^1\hat{R} + LG_0^{-1}\hat{L}\right)$ for an intermodal phase of $\alpha = 0$ (radial polarization), $\alpha = \frac{\pi}{6}$(spiral polarization), and $\alpha = \pi$ (azimuthal polarization).

The Laguerre-Gauss vector beams were generated experimentally and simulated numerically. Two different approaches were explored: first the same vector mode was generated but the intermodal phase was modified; secondly, different values for the radial and azimuthal indexes, related with the topological charge and number of rings respectively, were explored. Without loss of generality, the analysis will be restricted to the Laguerre-Gauss vector modes $\frac{\sqrt{2}}{2}\left(LG_0^1\hat{R} + LG_0^{-1}\hat{L}\right)$, $\frac{\sqrt{2}}{2}\left(LG_2^1\hat{R} + LG_2^{-1}\hat{L}\right)$ and $\frac{\sqrt{2}}{2}\left(LG_1^3\hat{R} + LG_1^{-3}\hat{L}\right)$.

On figure 6.1 scalar modes LG with the same number of rings and opposite topological charge were superimposed to generate the vector mode $\frac{\sqrt{2}}{2}\left(LG_0^1\hat{R} + LG_0^{-1}\hat{L}\right)$, but the intermodal phase was computationally modified to have radial ($\alpha = 0$), spiral ($\alpha = \frac{\pi}{6}$) and azimuthal polarisation ($\alpha = \pi$). The four experimental measurements for intensity are shown and compared with the numerical simulation and, as can be seen, there is a good agreement between both: for I_H and I_D there is a distribution showing two petals orientated in a different direction in accordance with the intermodal phase and the orientation of the linear polarizer; on the other hand, I_R and I_L show an almost homogeneous donut-like distribution although in the experimental measurements I_R is more intense than I_L, which could be due to a wrong angle in any of the optical elements used in the generation or the detection, while for the simulation both have the same intensity.

When exploring different topological charges and number of rings, it is found that I_H and I_D have the same form in the numerical simulation and experiment while for I_R and I_L there are differences regarding the homogeneity of the distribution, which

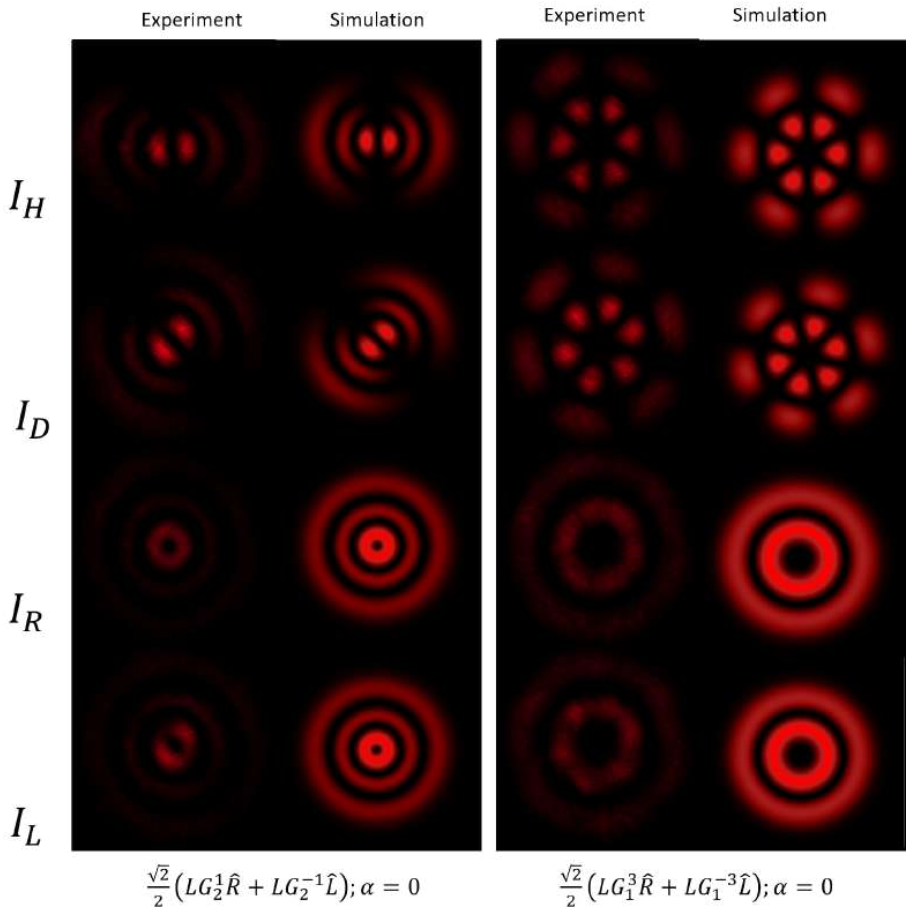

FIGURE 6.2: Vector modes for an intermodal phase of $\alpha = 0$ in both cases.

are more evident in the case of a topological charge $l = 3$, and in general as the topological charge increases, so does the distortion of the intensity distribution. On the other hand, it is worth to notice that the intensity of the rings decreases radially dramatically in the experiment while in the numerical simulation it remains almost the same, that is, the variations in intensity are small; the discrepancies may be related with the fact that in the numerical simulation, a set of assumptions are made which may not match fully or exactly with the experimental conditions, for instance in the simulation factors such as imperfections in the optical devices, loses in the optical system, and diffractive effects are not considered into account, neither the possible measurement errors or calibration problems, since in the numerical simulation the ideal case is the one considered. The four intensity measurements for modes $\frac{\sqrt{2}}{2}\left(LG_2^1\hat{R} + LG_2^{-1}\hat{L}\right)$ and $\frac{\sqrt{2}}{2}\left(LG_1^3\hat{R} + LG_1^{-3}\hat{L}\right)$, as well as the numerical simulation, can be seen on figure 6.2.

6.2 Polarization reconstruction.

The intensity measurements were used to calculate Stokes parameters according with Stokes polarimetry as explained in the previous chapters; afterwards the polarization for the generated beams was reconstructed. It is possible to notice in figures 6.3 and 6.4 that the Stokes parameter S_0 is a ring with homogeneous distribution for

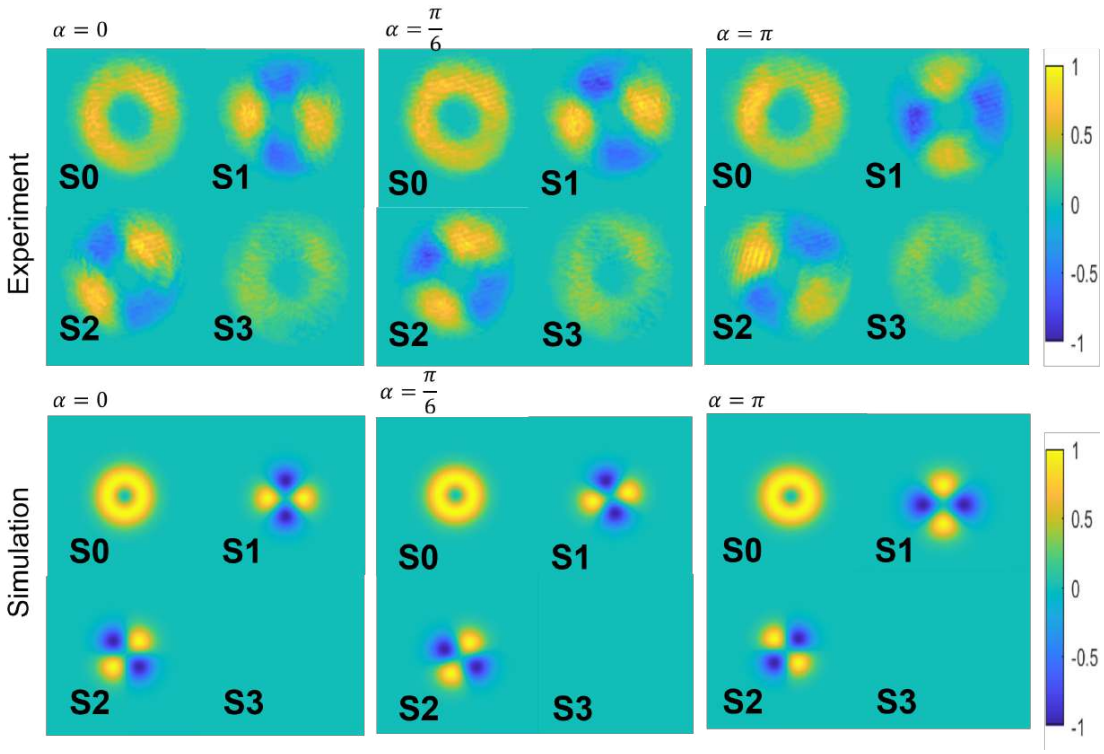

FIGURE 6.3: Stokes parameters for the vector mode $\frac{\sqrt{2}}{2}\left(LG_0^1\hat{R} + LG_0^{-1}\hat{L}\right)$ with different values for the intermodal phase.

the case of the mode $\frac{\sqrt{2}}{2}\left(LG_0^1\hat{R} + LG_0^{-1}\hat{L}\right)$, the parameters S_1 and S_2 have the same shape but different orientation and S_3 is not zero for any of the experimental cases while it is for the numerical simulations. In this case, the discrepancies may also be related with the differences between the numerical simulation and the experimental implementation, specially the characteristics of the camera play and important role since is in this stage where its sensitivity, calibration, alignment, and quality may give raise to artifacts, or the detection of noise and background light.

For the other two modes, namely $\frac{\sqrt{2}}{2}\left(LG_2^1\hat{R} + LG_2^{-1}\hat{L}\right)$ and $\frac{\sqrt{2}}{2}\left(LG_1^3\hat{R} + LG_1^{-3}\hat{L}\right)$, the parameter S_0 is a series of concentric rings, where, as expected, the number of rings corresponds with the radial index, as in the previous case; the distribution of the S_1 and S_2 Stokes' parameters is the same in both the experimental measurements and the simulation, though in the simulation it has higher values; finally, as in the previous case, the parameter S_3 is not zero for the experimental cases, but it is for the numerical simulation.

Once the Stokes parameters were measured, it was possible to use them, as explained on the previous chapter, to reconstruct the polarization states of each vector mode for regularly spaced points on a grid along its transverse plane. On figures 6.5 and 6.6 the polarization state is overlapped on the reconstructed intensity profile of the beams. On the figures the green ellipses correspond to circular-left handed polarization; the white lines to linear polarization and the orange ellipses to circular right-handed polarization.

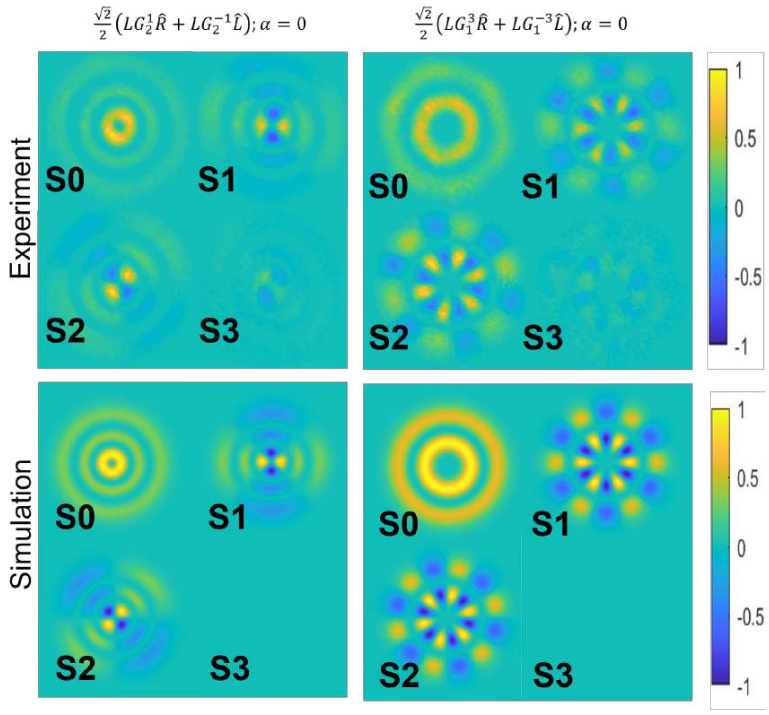

FIGURE 6.4: Stokes parameters for two vector modes for an intermodal phase $\alpha = 0$.

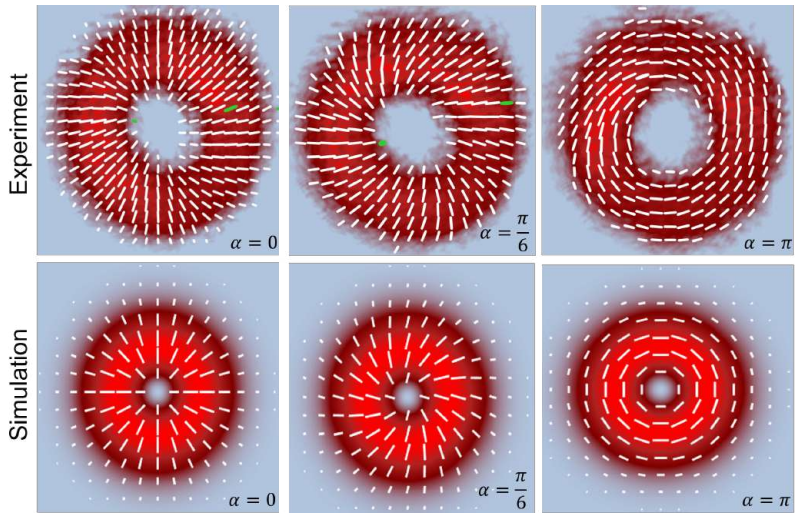

FIGURE 6.5: Polarization reconstruction for the LG beam with radial, spiral and azimuthal polarization states.

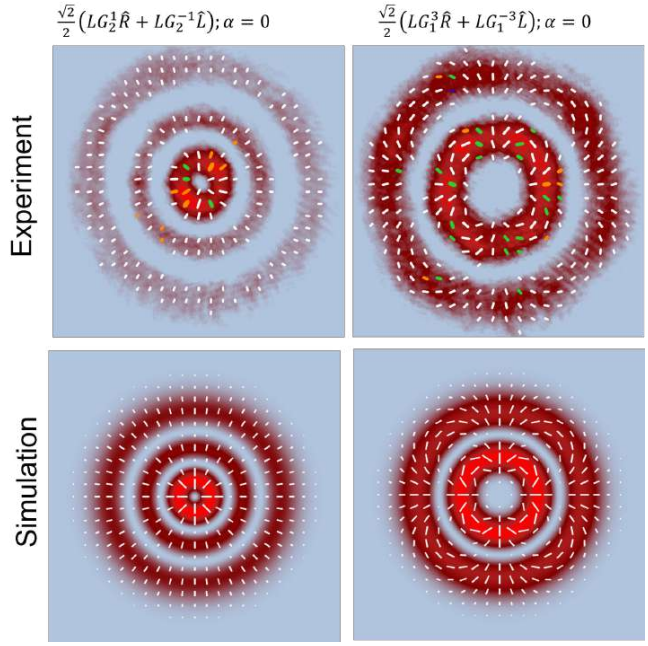

FIGURE 6.6: Polarization reconstruction for two different LG vector beams.

6.3 Purity analysis.

As mentioned above, the vectorness determines the "purity" of the generated modes, a value of 0 corresponds to a fully scalar beam and a value of 1 belongs to a fully vector beam. Therefore the Stokes parameters were used to compute vectornes using the expression 2.35:

$$C = \sqrt{1 - \frac{\mathbb{S}_1^2}{\mathbb{S}_0^2} - \frac{\mathbb{S}_2^2}{\mathbb{S}_0^2} - \frac{\mathbb{S}_3^2}{\mathbb{S}_0^2}} \tag{6.1}$$

where $\mathbb{S}_i$ corresponds to the values of the Stokes parameters S_i integrated over the whole transverse profile of the beam:

$$\mathbb{S}_i = \int \int_{-\infty}^{\infty} S_i dA; i = 0, 1, 2, 3 \tag{6.2}$$

The values obtained for the cases at hand, namely $\frac{\sqrt{2}}{2}\left(LG_0^1\hat{R} + LG_0^{-1}\hat{L}\right)$ with different intermodal phase (corresponding to radial, spiral and azimuthal polarization), $\frac{\sqrt{2}}{2}\left(LG_2^1\hat{R} + LG_2^{-1}\hat{L}\right)$ and $\frac{\sqrt{2}}{2}\left(LG_1^3\hat{R} + LG_1^{-3}\hat{L}\right)$ are summarized on table 6.1. Notice that most of the values are close to 1, in fact the furthest value corresponds to 0.89, indicating that the purity of the beams is very high. In all cases there is agreement between the theoretical and the calculated value, with percent error ranging from 3% to 11%. Therefore, as proposed by the technique, the generated beams posses high purity.

Vector mode	C_T	C_{E1}	C_{E2}	C_{E3}
$\frac{\sqrt{2}}{2}\left(LG_0^1\hat{R}+LG_0^{-1}\hat{L}\right), \alpha = 0.$	1.00	0.97	0.96	0.97
$\frac{\sqrt{2}}{2}\left(LG_0^1\hat{R}+LG_0^{-1}\hat{L}\right), \alpha = \frac{\pi}{6}.$	1.00	0.89	0.90	0.89
$\frac{\sqrt{2}}{2}\left(LG_0^1\hat{R}+LG_0^{-1}\hat{L}\right), \alpha = \pi.$	1.00	0.97	0.89	0.91
$\frac{\sqrt{2}}{2}\left(LG_2^1\hat{R}+LG_2^{-1}\hat{L}\right), \alpha = 0.$	1.00	0.95	0.93	0.95
$\frac{\sqrt{2}}{2}\left(LG_1^3\hat{R}+LG_1^{-3}\hat{L}\right), \alpha = 0.$	1.00	0.96	0.90	0.96

TABLE 6.1: Theoretical (C_T)and experimental (C_{Ei}) concurrence for the generated vector modes at different times.

6.4 Stability analysis

In the case of the $\frac{\sqrt{2}}{2}\left(LG_0^1\hat{R}+LG_0^{-1}\hat{L}\right)$ radial, spiral and azimuthal modes, a stability analysis was performed. First the ellipticity and the orientation of polarization for each point along the plane perpendicular to beam propagation were calculated at three different times considering; t_0 the first measurement, t_1 the second measurement, and t_2 the third measurement. For each measurement, the acquisition of four intensity images, as described on the previous chapter, were performed. The time difference between each measurement was of ten minutes.

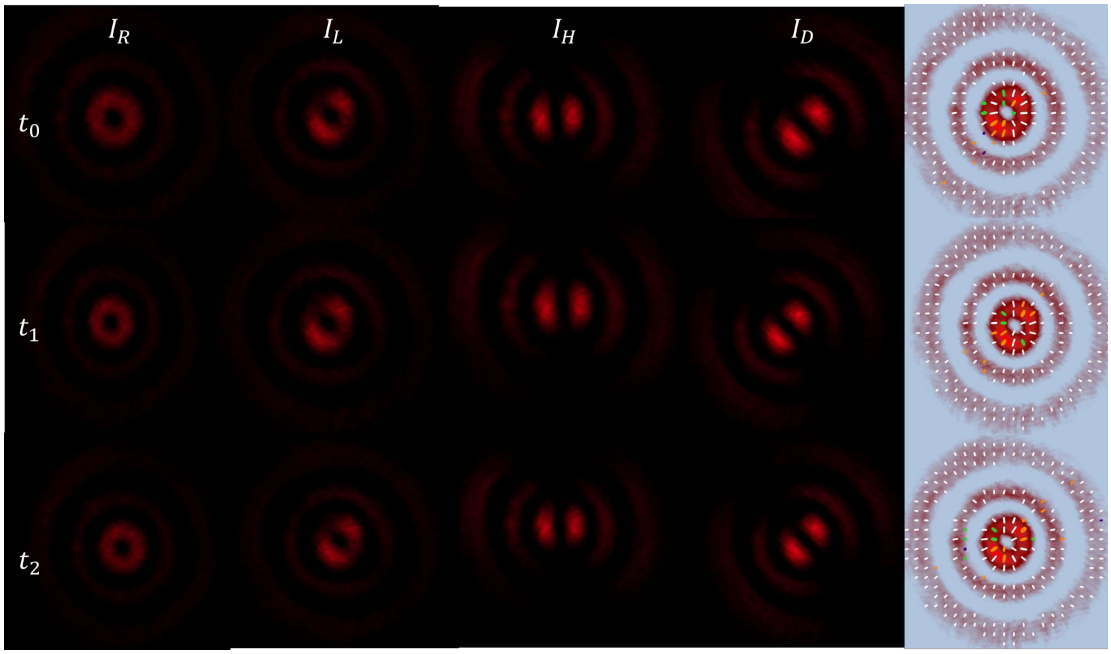

FIGURE 6.7: Intensity measurements and polarization reconstruction (last column) for the mode $\frac{\sqrt{2}}{2}\left(LG_2^1\hat{R}+LG_2^{-1}\hat{L}\right)$ at three different times.

Observe in image 6.7 the intensity measurements and polarization reconstruction for the mode $\frac{\sqrt{2}}{2}\left(LG_2^1\hat{R}+LG_2^{-1}\hat{L}\right)$ at three different times. By the first qualitative inspection, the intensity distributions and the polarization reconstruction have a remarkable similarity, in fact it is difficult to point a particular difference. However,

upon subjecting the images to meticulous scrutiny as explained on chapter 2 and following the methodology described by Perez-Garcia and collaborators in [21], the root mean squared error (RMSE) of both parameters for each polarization ellipse across the transverse plane was calculated to make a quantitative comparison between the values obtained at t_0 in contrast to the values obtained for $t = t_1$ and $t = t_2$.

Vector mode	azimuthal		spiral		radial	
	t_0 vs t_1	t_0 vs t_2	t_0 vs t_1	t_0 vs t_2	t_0 vs t_1	t_0 vs t_2
$RMSE_\alpha$	1.3317%	1.7768%	0.8427%	1.2715%	1.4122%	1.7721%
$RMSE_f$	0.0007%	0.0016%	0.0012%	0.0006%	0.0023%	0.0036%

TABLE 6.2: $RMSE_\alpha$ y $RMSE_f$ of the modes for azimuthal, spiral, and radial $\frac{\sqrt{2}}{2}\left(LG_0^1\hat{R} + LG_0^{-1}\hat{L}\right)$ mode .

As can be seen on table 6.2 the RMSE for all the cases is less than 2% indicating a high similarity among the three measurements. Since the comparison is made between the same beam at different times, the values obtained for RMSE show that the beam is very similar to itself over time, with any differences being minor (observe in figure 6.8 an example of this), and perhaps caused by small fluctuations in the measurement devices, the methodology followed for data acquisition or calibration errors in the devices used in the experimental setup. As it has been highlighted in previous chapters, there is not a consensus about a quantitative measurement to determine and classify the stability of the beams; in this sense, this is a pioneer work which gives a first approach that can provide a first step for a more precise classification of the stability in a vector beam. In spite of the latter and with careful consideration, it is possible to conclude that the fluctuations in the intermodal phase are likely negligible and the generated beams are highly stable.

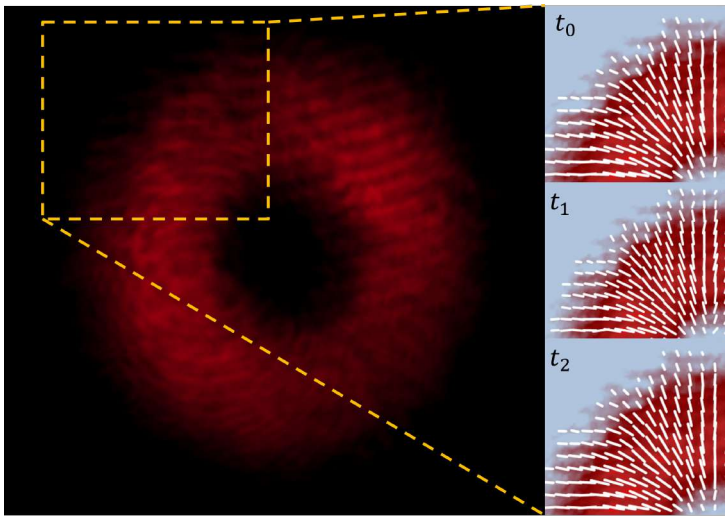

FIGURE 6.8: Detail of the polarization and intensity distribution for a section of the beam $\frac{\sqrt{2}}{2}\left(LG_0^1\hat{R} + LG_0^{-1}\hat{L}\right)$ at three different times.

Chapter 7

Conclusions and further work

As the interest in exploring structured light has increased, a bunch of unseen properties, behaviors and applications have been found, such as the mentioned in the previous chapters, which include the self-healing property [8] or the property of having orbital angular momentum [9] on the one side, and applications ranging from optical [11, 12, 13], to biomedical [37, 68]. At the same time, this interest triggered the development of technological advances and a great progress in the field of structured light, as presented in [10].

Some of the areas in which structured light have found interesting applications include optical tweezers, metrology, high resolution microscopy, optical communications, among others. Among the needs of the field, looking for generation and characterization techniques has been medular and in this context the use of SLMs has gained prominence since this devices enables the creation of light beams with virtually any desired shape. In spite of the broad number of current techniques for the generation of structured light, generating vector beams that at the same time posses high purity and stability has not been achieved. In fact there is not consensual well-established method for evaluating the stability of the generated beams over time and the approaches are generally based on qualitative descriptions rather than quantitative approximations. This work explored the use of a spatial light modulator in a configuration that has not been previously used in the field and provides a quantitative means for evaluating the stability of the generated beams.

The conclusions that can be derived from this work are as follows: first of all the apparent disadvantage of SLMs which is its polarization-sensitive attribute was the key to achieve generation of vector beams on-axis and therefore ensuring that the two polarization components follow always the same optical path and the intermodal phase remains constant over time. It was possible to generate LG vector beams by combining Laguerre-Gauss scalar modes with the same number of rings and opposite topological charges. It was further demonstrated that the vector modes generated posses a high degree of purity and are highly stable. This was done by calculating its concurrence (degree of non-separability between the spatial and polarisation degrees of freedom), flatness and orientation of the reconstructed polarization ellipses of the whole transverse plane, and comparing these values for measurements of the same beam in different times by calculating the root mean squared error and finding errors below 2% in all cases. The small discrepancies may be explained by problems related to the measurement technique, imperfections in the optical elements used, and tiny deviations in calibration rather than by the quality of the generation technique proposed.

As a proof-of-principle for the proposed technique, we focused on the generation of LG beams, nevertheless the same principle may be followed to generate other beams with arbitrary polarization distributions and spatial shapes. Although some aspects are still to be improved to enhance the scope of the technique demonstrated. Further work include rethink on how the setup may be modified to achieve complex amplitude modulation in both halves of the spatial light modulator, and the generalization of the technique to generate other families of modes. Additionally it would be possible to explore more deeply a way of quantitative characterizing the stability of vector beams and even propose a classification. An alternative route to take in the future is the use of this highly stable beams in a specific application, for example in optical metrology or optical tweezers and refine the technique to achieve the best generation of the target vector beam.

Bibliography

[1] A. Forbes, M. de Oliveira, and M. R. Dennis. "Structured light". In: *Nature Photonics* 15.4 (Mar. 2021), pp. 253–262. DOI: 10.1038/s41566-021-00780-4. URL: https://doi.org/10.1038/s41566-021-00780-4.

[2] A. Forbes. "Structured Light: Tailored for Purpose". In: *Optics and Photonics News* 31.6 (June 2020), p. 24. DOI: 10.1364/opn.31.6.000024. URL: https://doi.org/10.1364/opn.31.6.000024.

[3] O. Angelsky et al. "Structured Light: Ideas and Concepts". In: *Frontiers in Physics* 8 (May 2020). DOI: 10.3389/fphy.2020.00114. URL: https://doi.org/10.3389/fphy.2020.00114.

[4] A. Forbes. *How to shape light with applications*. Elsevier, 2008. DOI: 10.1016/b978-0-12-374027-4.x0001-1. URL: https://doi.org/10.1016/b978-0-12-374027-4.x0001-1.

[5] C. Rosales-Guzmán and A. Forbes. *How to Shape Light with Spatial Light Modulators*. SPIE PRESS, 2017. DOI: 10.1117/3.2281295. URL: https://doi.org/10.1117/3.2281295.

[6] B. Ndagano C. Rosales-Guzmán and A. Forbes. "A review of complex vector light fields and their applications". In: *Journal of Optics* 20.12 (Nov. 2018), p. 123001. DOI: 10.1088/2040-8986/aaeb7d. URL: https://doi.org/10.1088/2040-8986/aaeb7d.

[7] M. Giovani. "Vector beams for fundamental physics and applications". PhD thesis. City University of New York, 2016.

[8] I. Nape Y. Shen S. Pidishety and A. Dudley. "Self-healing of structured light: a review". In: *Journal of Optics* 24.10 (Sept. 2022), p. 103001. DOI: 10.1088/2040-8986/ac8888. URL: https://doi.org/10.1088/2040-8986/ac8888.

[9] J. Courtial M. Padgett and L. Allen. "Light's Orbital Angular Momentum". In: *Physics Today* 57.5 (May 2004), pp. 35–40. DOI: 10.1063/1.1768672. URL: https://doi.org/10.1063/1.1768672.

[10] H. Rubinsztein-Dunlop et al. "Roadmap on structured light". In: *Journal of Optics* 19.1 (2016), p. 013001. DOI: 10.1088/2040-8978/19/1/013001. URL: https://doi.org/10.1088/2040-8978/19/1/013001.

[11] H. Moradi et al. "Efficient optical trapping with cylindrical vector beams". In: *Optics Express* 27.5 (Feb. 2019), p. 7266. DOI: 10.1364/oe.27.007266. URL: https://doi.org/10.1364/oe.27.007266.

[12] O. Angelsky et al. "On polarization metrology (estimation) of the degree of coherence of optical waves". In: *Optics Express* 17.18 (Aug. 2009), p. 15623. DOI: 10.1364/oe.17.015623. URL: https://doi.org/10.1364/oe.17.015623.

[13] M. Liu et al. "Super-resolution optical microscopy using cylindrical vector beams". In: *Nanophotonics* 11.15 (June 2022), pp. 3395–3420. DOI: 10.1515/nanoph-2022-0241. URL: https://doi.org/10.1515/nanoph-2022-0241.

[14] B. Ndagano et al. "Creation and Detection of Vector Vortex Modes for Classical and Quantum Communication". In: *Journal of Lightwave Technology* 36.2

(Jan. 2018), pp. 292–301. DOI: 10.1109/jlt.2017.2766760. URL: https://doi.org/10.1109/jlt.2017.2766760.

[15] J. Wang. "Advances in communications using optical vortices". In: *Photonics Research* 4.5 (Sept. 2016), B14. DOI: 10.1364/prj.4.000b14. URL: https://doi.org/10.1364/prj.4.000b14.

[16] J. Wang and Y. Liang. "Generation and Detection of Structured Light: A Review". In: *Frontiers in Physics* 9 (May 2021). DOI: 10.3389/fphy.2021.688284. URL: https://doi.org/10.3389/fphy.2021.688284.

[17] J. Bougrenet-de-la-Tocnaye and L. Dupont. "Complex amplitude modulation by use of liquid-crystal spatial light modulators". In: *Applied Optics* 36.8 (Mar. 1997), p. 1730. DOI: 10.1364/ao.36.001730. URL: https://doi.org/10.1364/ao.36.001730.

[18] T. Konrad M. McLaren and A. Forbes. "Measuring the nonseparability of vector vortex beams". In: *Physical Review A* 92.2 (Aug. 2015). DOI: 10.1103/physreva.92.023833. URL: https://doi.org/10.1103/physreva.92.023833.

[19] B. Ndagano et al. "Beam quality measure for vector beams". In: *Optics Letters* 41.15 (July 2016), p. 3407. DOI: 10.1364/ol.41.003407. URL: https://doi.org/10.1364/ol.41.003407.

[20] A. Selyem et al. "Basis-independent tomography and nonseparability witnesses of pure complex vectorial light fields by Stokes projections". In: *Physical Review A* 100.6 (Dec. 2019). DOI: 10.1103/physreva.100.063842. URL: https://doi.org/10.1103/physreva.100.063842.

[21] R. Hernandez-Aranda B. Perez-Garcia C. López-Mariscal and J. Gutiérrez-Vega. "On-demand tailored vector beams". In: *Applied Optics* 56.24 (Aug. 2017), p. 6967. DOI: 10.1364/ao.56.006967. URL: https://doi.org/10.1364/ao.56.006967.

[22] B. Saleh and M. Teich. *Fundamentals of Photonics*. John Wiley & Sons, Inc., Aug. 1991. DOI: 10.1002/0471213748. URL: https://doi.org/10.1002/0471213748.

[23] A. Forbes, ed. *Laser Beam Propagation. Generation and propagation of customized light*. CRC Press, Feb. 2014.

[24] X. Hu. "Generation of new structured light fields and their applications in optical metrology". PhD thesis. Harbin University os Science and Technology, 2021.

[25] S. Derevyanko U. Levy and Y. Silberberg. "Light Modes of Free Space". In: *Progress in Optics*. Elsevier, 2016, pp. 237–281. DOI: 10.1016/bs.po.2015.10.001. URL: https://doi.org/10.1016/bs.po.2015.10.001.

[26] Q. Zhan. "Cylindrical vector beams: from mathematical concepts to applications". In: *Advances in Optics and Photonics* 1 (2009), pp. 1–57.

[27] E. J. Galvez. "Vector beams in free space". In: *The Angular Momentum of Light*. Cambridge University Press, Nov. 2012, pp. 51–70. DOI: 10.1017/cbo9780511795213.004. URL: https://doi.org/10.1017/cbo9780511795213.004.

[28] N. Fontaine et al. "Laguerre-Gaussian mode sorter". In: *Nature Communications* 10.1 (Apr. 2019). DOI: 10.1038/s41467-019-09840-4. URL: https://doi.org/10.1038/s41467-019-09840-4.

[29] Y. Li Y. Yang and C. Wang. "Generation and expansion of Laguerre–Gaussian beams". In: *Journal of Optics* 51.4 (May 2022), pp. 910–926. DOI: 10.1007/s12596-022-00857-5. URL: https://doi.org/10.1007/s12596-022-00857-5.

[30] L. Allen A. Neil I. MacVicar and M. Padgett. "Intrinsic and Extrinsic Nature of the Orbital Angular Momentum of a Light Beam". In: *Physical Review Letters* 88.5 (Jan. 2002). DOI: 10.1103/physrevlett.88.053601. URL: https://doi.org/10.1103/physrevlett.88.053601.

[31] S. Kennedy et al. "Creation of Laguerre-Gaussian laser modes using diffractive optics". In: *Physical Review A* 66.4 (Oct. 2002). DOI: 10.1103/physreva.66.043801. URL: https://doi.org/10.1103/physreva.66.043801.

[32] J. Lee et al. "Laguerre-Gauss and Hermite-Gauss soft X-ray states generated using diffractive optics". In: *Nature Photonics* 13.3 (Jan. 2019), pp. 205–209. DOI: 10.1038/s41566-018-0328-8. URL: https://doi.org/10.1038/s41566-018-0328-8.

[33] R. Spreeuw L. Allen M. Beijersbergen and J. Woerdman. "Orbital angular momentum of light and the transformation of Laguerre-Gaussian laser modes". In: *Physical Review A* 45.11 (June 1992), pp. 8185–8189. DOI: 10.1103/physreva.45.8185. URL: https://doi.org/10.1103/physreva.45.8185.

[34] P. Török and P. Munro. "The use of Gauss-Laguerre vector beams in STED microscopy". In: *Optics Express* 12.15 (July 2004), p. 3605. DOI: 10.1364/opex.12.003605. URL: https://doi.org/10.1364/opex.12.003605.

[35] S. Chen et al. "Generation of arbitrary cylindrical vector beams on the higher order Poincaré sphere". In: *Optics Letters* 39.18 (Sept. 2014), p. 5274. DOI: 10.1364/ol.39.005274. URL: https://doi.org/10.1364/ol.39.005274.

[36] E. J. Galvez. "Vector beams in free space". In: *The Angular Momentum of Light*. Cambridge University Press, Nov. 2012, pp. 51–70. DOI: 10.1017/cbo9780511795213.004. URL: https://doi.org/10.1017/cbo9780511795213.004.

[37] I. Moreno and M. Sánchez-López. "Generation and detection of vector beams with geometric phase components and spatial light modulators". In: *Polarized Light and Optical Angular Momentum for Biomedical Diagnostics*. Ed. by J. Ramella-Roman et al. SPIE, Mar. 2021. DOI: 10.1117/12.2578490. URL: https://doi.org/10.1117/12.2578490.

[38] X. Hu and C. Rosales-Guzmán. "Generation and characterization of complex vector modes with digital micromirror devices: a tutorial". In: *Journal of Optics* 24.3 (Jan. 2022), p. 034001. DOI: 10.1088/2040-8986/ac4671. URL: https://doi.org/10.1088/2040-8986/ac4671.

[39] V. Kleiner A. Niv G. Biener and E. Hasman. "Spiral phase elements obtained by use of discrete space-variant subwavelength gratings". In: *Optics Communications* 251.4-6 (July 2005), pp. 306–314. DOI: 10.1016/j.optcom.2005.03.002. URL: https://doi.org/10.1016/j.optcom.2005.03.002.

[40] V. Kleiner G. Biener A. Niv and E. Hasman. "Formation of helical beams by use of Pancharatnam–Berry phase optical elements". In: *Optics Letters* 27.21 (Nov. 2002), p. 1875. DOI: 10.1364/ol.27.001875. URL: https://doi.org/10.1364/ol.27.001875.

[41] J. A. Davis et al. "Two-dimensional polarization encoding with a phase-only liquid-crystal spatial light modulator". In: *Applied Optics* 39.10 (Apr. 2000), p. 1549. DOI: 10.1364/ao.39.001549. URL: https://doi.org/10.1364/ao.39.001549.

[42] E. Otte C. Alpmann C. Schlickriede and C. Denz. "Dynamic modulation of Poincaré beams". In: *Scientific Reports* 7.1 (Aug. 2017). DOI: 10.1038/s41598-017-07437-9. URL: https://doi.org/10.1038/s41598-017-07437-9.

[43] C. Manzo L. Marrucci and D. Paparo. "Optical Spin-to-Orbital Angular Momentum Conversion in Inhomogeneous Anisotropic Media". In: *Physical Review Letters* 96.16 (Apr. 2006). DOI: 10.1103/physrevlett.96.163905. URL: https://doi.org/10.1103/physrevlett.96.163905.

[44] A. Rubano et al. "Q-plate technology: a progress review [Invited]". In: *Journal of the Optical Society of America B* 36.5 (Feb. 2019), p. D70. DOI: 10.1364/josab.36.000d70. URL: https://doi.org/10.1364/josab.36.000d70.

[45] R. Devlin et al. "Arbitrary spin-to-orbital angular momentum conversion of light". In: *Science* 358.6365 (Nov. 2017), pp. 896–901. DOI: 10.1126/science.aao5392. URL: https://doi.org/10.1126/science.aao5392.

[46] X. Wang K. Zeng S. He and H. Luo. "Generation of Vector Vortex Beams Based on the Optical Integration of Dynamic Phase and Geometric Phase". In: *Photonics* 10.2 (Feb. 2023), p. 214. DOI: 10.3390/photonics10020214. URL: https://doi.org/10.3390/photonics10020214.

[47] C. Maurer et al. "Tailoring of arbitrary optical vector beams". In: *New Journal of Physics* 9.3 (Mar. 2007), pp. 78–78. DOI: 10.1088/1367-2630/9/3/078. URL: https://doi.org/10.1088/1367-2630/9/3/078.

[48] E. Wolf. *Introduction to the theory of coherence and polarization of light*. Cambridge University Press, 2007.

[49] D. Goldstein. *Polarized light*. Marcel Dekker, Inc, 2003.

[50] A. Kumar and A. Ghatak. "The Stokes Parameters Representation". In: *Polarization of Light with Applications in Optical Fibers*. SPIE, 2011, pp. 97–119. DOI: 10.1117/3.861761.ch6. URL: https://doi.org/10.1117/3.861761.ch6.

[51] B. Schaefer et al. "Measuring the Stokes polarization parameters". In: *American Journal of Physics* 75.2 (Feb. 2007), pp. 163–168. DOI: 10.1119/1.2386162. URL: https://doi.org/10.1119/1.2386162.

[52] H. Sroor et al. "Purity of Vector Vortex Beams through a Birefringent Amplifier". In: *Physical Review Applied* 9.4 (Apr. 2018). DOI: 10.1103/physrevapplied.9.044010. URL: https://doi.org/10.1103/physrevapplied.9.044010.

[53] I. Nape et al. "Vector-Mode Decay in Atmospheric Turbulence: An Analysis Inspired by Quantum Mechanics". In: *Physical Review Applied* 15.3 (Mar. 2021). DOI: 10.1103/physrevapplied.15.034030. URL: https://doi.org/10.1103/physrevapplied.15.034030.

[54] J. Huguenin C. Borges M. Hor-Meyll and A. Khoury. "Bell-like inequality for the spin-orbit separability of a laser beam". In: *Physical Review A* 82.3 (Sept. 2010). DOI: 10.1103/physreva.82.033833. URL: https://doi.org/10.1103/physreva.82.033833.

[55] B. Jack et al. "Precise quantum tomography of photon pairs with entangled orbital angular momentum". In: *New Journal of Physics* 11.10 (Oct. 2009), p. 103024. DOI: 10.1088/1367-2630/11/10/103024. URL: https://doi.org/10.1088/1367-2630/11/10/103024.

[56] G. Crawford R. Ondris-Crawford and J. Doane. "The phase of the future". In: *The Physics Teacher* 30.6 (Sept. 1992), pp. 332–339. DOI: 10.1119/1.2343568. URL: https://doi.org/10.1119/1.2343568.

[57] P. Gennes and J. Prost. *The Physics of Liquid Crystals*. Clarendon Press, 1995.

[58] P. Collings. *Liquid Crystals: Nature's Delicate Phase Of Matter*. Princeton University Press, 2002.

[59] M. Malik et al. "Overview of Liquid Crystal Research: Computational Advancements, Challenges, Future Prospects and Applications". In: *Liquid Crystals*. IntechOpen, Aug. 2022. DOI: 10.5772/intechopen.101417. URL: https://doi.org/10.5772/intechopen.101417.

[60] N. Vaupotic J. Pavlin and M. Cepic. "Liquid crystals: a new topic in physics for undergraduates". In: *European Journal of Physics* 34.3 (Apr. 2013), pp. 745–761. DOI: 10.1088/0143-0807/34/3/745. URL: https://doi.org/10.1088/0143-0807/34/3/745.

[61] I. Carlescu. "Introductory Chapter: Liquid Crystals". In: *Liquid Crystals - Self-Organized Soft Functional Materials for Advanced Applications*. IntechOpen, Jan. 2019. DOI: 10.5772/intechopen.82296. URL: https://doi.org/10.5772/intechopen.82296.

[62] R. Ondris-Crawford G. Crawford. "Liquid crystal displays: molecules at work". In: *Physics Education* 29.5 (Sept. 1994), pp. 307–312. DOI: 10.1088/0031-9120/29/5/008. URL: https://doi.org/10.1088/0031-9120/29/5/008.

[63] Y. Naka T. Sasaki K. Van Le and T. Sassa. "The Photorefractive Effect in Liquid Crystals". In: *Liquid Crystals - Self-Organized Soft Functional Materials for Advanced Applications*. IntechOpen, Jan. 2019. DOI: 10.5772/intechopen.81573. URL: https://doi.org/10.5772/intechopen.81573.

[64] B. Boruah. "Dynamic manipulation of a laser beam using a liquid crystal spatial light modulator". In: *American Journal of Physics* 77.4 (Apr. 2009), pp. 331–336. DOI: 10.1119/1.3054349. URL: https://doi.org/10.1119/1.3054349.

[65] Z. You Z. Zhang and D. Chu. "Fundamentals of phase-only liquid crystal on silicon (LCOS) devices". In: *Light: Science &amp Applications* 3.10 (Oct. 2014), e213–e213. DOI: 10.1038/lsa.2014.94. URL: https://doi.org/10.1038/lsa.2014.94.

[66] A. Kumar J. Prakash and S. Chauhan. "Aligning Liquid Crystal Materials through Nanoparticles: A Review of Recent Progress". In: *Liquids* 2.2 (June 2022), pp. 50–71. DOI: 10.3390/liquids2020005. URL: https://doi.org/10.3390/liquids2020005.

[67] A. Sengupta. "Topological microfluidics: present and prospects". In: *Liquid Crystals Today* 24.3 (May 2015), pp. 70–80. DOI: 10.1080/1358314x.2015.1039196. URL: https://doi.org/10.1080/1358314x.2015.1039196.

[68] Y. Dong and Z. Yang. "Beyond displays: The recent progress of liquid crystals for bio/chemical detections". In: *Chinese Science Bulletin* 58.21 (Apr. 2013), pp. 2557–2562. DOI: 10.1007/s11434-013-5767-5. URL: https://doi.org/10.1007/s11434-013-5767-5.

[69] L. Zhu and J. Wang. "Arbitrary manipulation of spatial amplitude and phase using phase-only spatial light modulators". In: *Scientific Reports* 4.1 (Dec. 2014). DOI: 10.1038/srep07441. URL: https://doi.org/10.1038/srep07441.

[70] A. Jullien. "Spatial light modulators". In: *Photoniques* 101 (Mar. 2020), pp. 59–64. DOI: 10.1051/photon/202010159. URL: https://doi.org/10.1051/photon/202010159.

[71] B. Boruah. "Dynamic manipulation of a laser beam using a liquid crystal spatial light modulator". In: *American Journal of Physics* 77.4 (Apr. 2009), pp. 331–336. DOI: 10.1119/1.3054349. URL: https://doi.org/10.1119/1.3054349.

[72] N. Savage. "Digital spatial light modulators". In: *Nature Photonics* 3.3 (Mar. 2009), pp. 170–172. DOI: 10.1038/nphoton.2009.18. URL: https://doi.org/10.1038/nphoton.2009.18.

[73] S. Bernet C. Maurer A. Jesacher and M. Ritsch-Marte. "What spatial light modulators can do for optical microscopy". In: *Laser &amp Photonics Reviews* 5.1 (Dec. 2010), pp. 81–101. DOI: 10.1002/lpor.200900047. URL: https://doi.org/10.1002/lpor.200900047.

[74] V. Tiwari and N. Bisht. "Spatial Light Modulators and Their Applications in Polarization Holography". In: *Holography - Recent Advances and Applications*.

IntechOpen, Feb. 2023. DOI: 10.5772/intechopen.107110. URL: https://doi.org/10.5772/intechopen.107110.

[75] A. Forbes, A. Dudley, and M. McLaren. "Creation and detection of optical modes with spatial light modulators". In: *Advances in Optics and Photonics* 8.2 (Apr. 2016), p. 200. DOI: 10.1364/aop.8.000200. URL: https://doi.org/10.1364/aop.8.000200.

[76] I. Moreno et al. "Efficient generation of vector beams". In: *Laser Beam Shaping XX*. Ed. by A. Dudley and A. Laskin. SPIE, Aug. 2020. DOI: 10.1117/12.2567768. URL: https://doi.org/10.1117/12.2567768.

[77] I. Vellekoop E. van-Putten and A. Mosk. "Spatial amplitude and phase modulation using commercial twisted nematic LCDs". In: *Applied Optics* 47.12 (Apr. 2008), p. 2076. DOI: 10.1364/ao.47.002076. URL: https://doi.org/10.1364/ao.47.002076.

[78] G. Méndez V. Arrizón and D. Sánchez-de-La-Llave. "Accurate encoding of arbitrary complex fields with amplitude-only liquid crystal spatial light modulators". In: *Optics Express* 13.20 (Oct. 2005), p. 7913. DOI: 10.1364/opex.13.007913. URL: https://doi.org/10.1364/opex.13.007913.

[79] D. Huang et al. "A low-cost spatial light modulator for use in undergraduate and graduate optics labs". In: *American Journal of Physics* 80.3 (Feb. 2012), pp. 211–215. DOI: 10.1119/1.3666834. URL: https://doi.org/10.1119/1.3666834.

[80] W.Duncan D. Dudley and J. Slaughter. "Emerging digital micromirror device (DMD) applications". In: *SPIE MOEMS-MEMS*. 2003.

[81] R. Lu Y. Ren and L. Gong. "Tailoring light with a digital micromirror device". In: *Annalen der Physik* 527.7-8 (July 2015), pp. 447–470. DOI: 10.1002/andp.201500111. URL: https://doi.org/10.1002/andp.201500111.

[82] F. Mecillas-Hernández B. Perez-Garcia and C. Rosales-Guzmán. "Highly-stable generation of vector beams through a common-path interferometer and a DMD". In: *Journal of Optics* 24.7 (June 2022), p. 074007. DOI: 10.1088/2040-8986/ac76d2. URL: https://doi.org/10.1088/2040-8986/ac76d2.

[83] F. Mecillas-Hernández. "Generación de haces vectoriales mediante dispositivos digitales de microespejos". MA thesis. Centro de Investigaciones en Óptica, A. C., 2022.

[84] S. Turtaev et al. "Comparison of nematic liquid-crystal and DMD based spatial light modulation in complex photonics". In: *Optics Express* 25.24 (Nov. 2017), p. 29874. DOI: 10.1364/oe.25.029874. URL: https://doi.org/10.1364/oe.25.029874.

[85] S. Ngcobo et al. "A digital laser for on-demand laser modes". In: *Nature Communications* 4.1 (Aug. 2013). DOI: 10.1038/ncomms3289. URL: https://doi.org/10.1038/ncomms3289.

[86] L. Burger an I. Litvin, S. Ngcobo, and A. Forbes. "Implementation of a spatial light modulator for intracavity beam shaping". In: *Journal of Optics* 17.1 (Dec. 2014), p. 015604. DOI: 10.1088/2040-8978/17/1/015604. URL: https://doi.org/10.1088/2040-8978/17/1/015604.

[87] K. Valadéz J. Davis and D. Cottrell. "Encoding amplitude and phase information onto a binary phase-only spatial light modulator". In: *Applied Optics* 42.11 (Apr. 2003), p. 2003. DOI: 10.1364/ao.42.002003. URL: https://doi.org/10.1364/ao.42.002003.

[88] M. A. A. Neil et al. "Method for the generation of arbitrary complex vector wave fronts". In: *Optics Letters* 27.21 (Nov. 2002), p. 1929. DOI: 10.1364/ol.27.001929. URL: https://doi.org/10.1364/ol.27.001929.

[89] C. Maurer et al. "Tailoring of arbitrary optical vector beams". In: *New Journal of Physics* 9.3 (Mar. 2007), pp. 78–78. DOI: 10.1088/1367-2630/9/3/078. URL: https://doi.org/10.1088%5C%2F1367-2630%5C%2F9%5C%2F3%5C%2F078.

[90] V. Arrizón et al. "Pixelated phase computer holograms for the accurate encoding of scalar complex fields". In: *Journal of the Optical Society of America A* 24.11 (Oct. 2007), p. 3500. DOI: 10.1364/josaa.24.003500. URL: https://doi.org/10.1364/josaa.24.003500.

[91] X. Wang J. Ding et al. "Generation of arbitrary vector beams with a spatial light modulator and a common path interferometric arrangement". In: *Optics Letters* 32.24 (Dec. 2007), p. 3549. DOI: 10.1364/ol.32.003549. URL: https://doi.org/10.1364/ol.32.003549.

[92] I. Moreno et al. "Complete polarization control of light from a liquid crystal spatial light modulator". In: *Optics Express* 20.1 (Dec. 2011), p. 364. DOI: 10.1364/oe.20.000364. URL: https://doi.org/10.1364/oe.20.000364.

[93] Z. Chen et al. "Complete shaping of optical vector beams". In: *Optics Express* 23.14 (June 2015), p. 17701. DOI: 10.1364/oe.23.017701. URL: https://doi.org/10.1364/oe.23.017701.

[94] C. Rosales-Guzmán, N. Bhebhe, and A. Forbes. "Simultaneous generation of multiple vector beams on a single SLM". In: *Optics Express* 25.21 (Oct. 2017), p. 25697. DOI: 10.1364/oe.25.025697. URL: https://doi.org/10.1364/oe.25.025697.

[95] E. Otte, K. Tekce, and C. Denz. "Spatial multiplexing for tailored fully-structured light". In: *Journal of Optics* 20.10 (Sept. 2018), p. 105606. DOI: 10.1088/2040-8986/aadef3. URL: https://doi.org/10.1088/2040-8986/aadef3.

[96] D. Gabor. "A New Microscopic Principle". In: *Nature* 161.4098 (May 1948), pp. 777–778. DOI: 10.1038/161777a0. URL: https://doi.org/10.1038/161777a0.

[97] P. Salter and M. Booth. "Adaptive optics in laser processing". In: *Light: Science &amp Applications* 8.1 (Nov. 2019). DOI: 10.1038/s41377-019-0215-1. URL: https://doi.org/10.1038/s41377-019-0215-1.

[98] V. Kesaev and A. Kiselev. "Phase-only modulation of light". In: *Optics Letters* 45.24 (Dec. 2020), p. 6703. DOI: 10.1364/ol.410450. URL: https://doi.org/10.1364/ol.410450.

[99] E. Bolduc et al. "Exact solution to simultaneous intensity and phase encryption with a single phase-only hologram". In: *Optics Letters* 38.18 (Sept. 2013), p. 3546. DOI: 10.1364/ol.38.003546. URL: https://doi.org/10.1364/ol.38.003546.

[100] T. Clark et al. "Comparison of beam generation techniques using a phase only spatial light modulator". In: *Optics Express* 24.6 (Mar. 2016), p. 6249. DOI: 10.1364/oe.24.006249. URL: https://doi.org/10.1364/oe.24.006249.

[101] T. Ando et al. "Mode purities of Laguerre–Gaussian beams generated via complex-amplitude modulation using phase-only spatial light modulators". In: *Optics Letters* 34.1 (Dec. 2008), p. 34. DOI: 10.1364/ol.34.000034. URL: https://doi.org/10.1364/ol.34.000034.

[102] D. Pi, J. Liu, and Y. Wang. "Review of computer-generated hologram algorithms for color dynamic holographic three-dimensional display". In: *Light: Science &amp Applications* 11.1 (July 2022). DOI: 10.1038/s41377-022-00916-3. URL: https://doi.org/10.1038/s41377-022-00916-3.

[103] H. Bartelt. "Computer-generated holographic component with optimum light efficiency". In: *Applied Optics* 23.10 (May 1984), p. 1499. DOI: 10.1364/ao.23.001499. URL: https://doi.org/10.1364/ao.23.001499.

[104] J. Kirsch D. Gregory and E. Tam. "Full complex modulation using liquid-crystal televisions". In: *Applied Optics* 31.2 (Jan. 1992), p. 163. DOI: 10.1364/ao.31.000163. URL: https://doi.org/10.1364/ao.31.000163.

[105] H. Miura J. Amako and T. Sonehara. "Wave-front control using liquid-crystal devices". In: *Applied Optics* 32.23 (Aug. 1993), p. 4323. DOI: 10.1364/ao.32.004323. URL: https://doi.org/10.1364/ao.32.004323.

[106] M. Hsieh. "Improvement of the complex modulated characteristic of cascaded liquid crystal spatial light modulators by using a novel amplitude compensated technique". In: *Optical Engineering* 46.7 (July 2007), p. 070501. DOI: 10.1117/1.2750658. URL: https://doi.org/10.1117/1.2750658.

[107] H. Hou et al. "Complex-amplitude single-pixel imaging using coherent structured illumination". In: *Optics Express* 29.25 (Dec. 2021), p. 41827. DOI: 10.1364/oe.443258. URL: https://doi.org/10.1364/oe.443258.

[108] J. Han Q. Gao J. Liu and X. Li. "Monocular 3D see-through head-mounted display via complex amplitude modulation". In: *Optics Express* 24.15 (July 2016), p. 17372. DOI: 10.1364/oe.24.017372. URL: https://doi.org/10.1364/oe.24.017372.

[109] A. Siemion et al. "Diffuserless holographic projection working on twin spatial light modulators". In: *Optics Letters* 37.24 (Dec. 2012), p. 5064. DOI: 10.1364/ol.37.005064. URL: https://doi.org/10.1364/ol.37.005064.

[110] V. Arrizón and D. Sánchez-de-la-Llave. "Double-phase holograms implemented with phase-only spatial light modulators: performance evaluation and improvement". In: *Applied Optics* 41.17 (June 2002), p. 3436. DOI: 10.1364/ao.41.003436. URL: https://doi.org/10.1364/ao.41.003436.

[111] C. Chang et al. "Speckle-suppressed phase-only holographic three-dimensional display based on double-constraint Gerchberg–Saxton algorithm". In: *Applied Optics* 54.23 (Aug. 2015), p. 6994. DOI: 10.1364/ao.54.006994. URL: https://doi.org/10.1364/ao.54.006994.

[112] G. Mínguez-Vega O. Mendoza-Yero and J. Lancis. "Encoding complex fields by using a phase-only optical element". In: *Optics Letters* 39.7 (Mar. 2014), p. 1740. DOI: 10.1364/ol.39.001740. URL: https://doi.org/10.1364/ol.39.001740.